

# CHAPTER - II

PREPARATION OF FERRITES, CHARACTERISATION AND FAR INFRARED STUDIES

## CHAPTER-II

## PREPARATION OF FERRITES, CHARACTERISATION AND FAR INFRARED STUDIES

## SECTION A : FERRITE PREPARATION

## 2.1 INTRODUCTION :

The chemical formula for magnetite or lodestone is  $\text{Fe}_3\text{O}_4$ , which more specifically can be written as  $\text{Fe}^{2+}\text{Fe}_2^{3+}\text{O}_4^{2-}$ . If divalent ferrous ion i.e.  $\text{Fe}^{2+}$  is replaced by another divalent metal ion such as Mn, Co, Ni, Cu, Mg, Zn or Cd, we get mixed ferrites. In general the chemical composition of ferrite is  $\text{Me}^{2+}\text{Fe}_2^{3+}\text{O}_4^{2-}$  where  $\text{Me}^{2+}$  is a divalent metal ion.

Ferrites are industrially important materials due to their peculiar magnetic and electric properties. The physical and chemical properties of ferrites fall into two categories viz. Intrinsic, related to constitution of ferrite and extrinsic, which are structure sensitive. Ferrite preparation needs heat treatment for formation of crystal structure of material. Heat treatment influences structural properties. The heat treatment like firing temperature, firing time, firing atmosphere rate of cooling cumulatively constitute the thermal history of sample through an imprint on all attendant microstructural parameters like grain size, defect concentration, porosity inclusions as well as orientation, size shape of grains.

## 2.2.1 PREPARATION OF FERRITES :

Simple, mixed and substitutional ferrites can be prepared by various methods.<sup>1,2,3</sup> Since ferrites are oxide magnetic materials, no special extraction involving molten phases is required. There

are two standard methods of ferrite preparation viz. ceramic method<sup>4,5,6</sup> and chemical method. In ceramic method it is possible to prepare complex chemical compositions with desired microstructure and shapes of final products much more economically than single crystals. Ceramics have sufficient mechanical strength which allows them to be moulded in desired shape. Ceramics provide a way of providing undesired effects such as eddy current losses, which can be suppressed by internal lamination along grain boundaries.<sup>7</sup> The majority of solids occurring in nature are polycrystalline rather than single crystals when special favourable conditions are not maintained the substance is found to consist a large number of separate grains whose sizes vary from  $10^3 \text{ \AA}^0$  to  $10^4 \text{ \AA}^0$ . Each grain is a crystal of irregular shape, because its growth is affected by adjacent crystals. Thus a polycrystalline body is composed of myriad of randomly oriented crystals. The consequent granular structure is called as polycrystalline structure.<sup>8</sup>

### 2.2.2 MECHANISM OF SOLID STATE REACTION :

Polycrystalline ferrites are usually formed by a solid state reaction between the starting materials such as oxides (or compounds such carbonates, nitrates, oxalates).

The homogeneous mixture of a metal oxide (MeO) and ferric oxide ( $\text{Fe}_2\text{O}_3$ ) are heated to an elevated temperature. The mechanism of solid state reaction is based on diffusion between divalent metal molecule Me and ferric oxide molecule  $\text{Fe}_2\text{O}_3$ .

Stage I :- In initial configuration there is only a single phase boundary between the reactants viz. divalent metal oxide MeO and ferric oxide.

Stage II :- After nucleation of ferrite, the boundary is replaced by two different phase boundaries, one phase boundary between metal oxide MeO and ferrite  $\text{MeFe}_2\text{O}_4$  and other between  $\text{Fe}_2\text{O}_3$  and  $\text{MeFe}_2\text{O}_4$ .

Stage III :- The reaction proceeds with transport of reactants through ferrite phase.

There are three different mechanism which attribute ferrite formation.

Mechanism I :- Only cations migrate in the opposite direction with the oxygen ions essentially stationary as suggested by Wagner<sup>9,10</sup>

Mechanism II :- Cation diffusion is compensated by an associated flux of anions instead of another cation migration.

Mechanism III :- Iron diffuses through ferrite layer in the reduced state  $\text{Fe}^{+2}$ . In such as case oxygen is transported through gaseous phase, being given off at  $\text{MeFe}_2\text{O}_4 / \text{Fe}_2\text{O}_3$  interface and are taken up again at MeO/  $\text{MeFe}_2\text{O}_4$  boundary.

### 2.2.3 STEPS IN FERRITE PREPARATION :

- 1 Preparation of material to form an intimate mixtures with the metal oxides in the required ratio in final product.

2. Presintering or calcination.
3. Powdering of presintered material and pressing it to form the required shape.
4. Sintering to form a final product.

#### 2.2.4 PREPARATION METHODS OF FERRITE COMPOSITION :

##### 2.2.4(a) Oxide method :

High purity metal oxides in the required proportion for final product are mixed together in stoichiometric proportion. They are mixed by wet milling for a long period with rotary steel balls for few hours. The mixture is dried and pressed into suitable shape before presintering and then finally sintered.

##### 2.2.4(b) Decomposition method :

Instead of oxides, carbonates (oxalates, nitrates) are mixed in requisite proportion and preheated in air, which produce oxide by thermal decomposition. The oxides so produced readily undergo a solid state reaction.<sup>10</sup> Other details are similar to oxide method.

##### 2.2.4(c) Hydroxide precipitation :

Economos<sup>11</sup> attempted to precipitate simultaneously the required hydroxide from a solution. The precipitate contain required metal ions in correct proportion already entimately mixed. Sato<sup>12</sup> and his co-workers prepared ultrafine spinel ferrites by this method.

#### 2.2.4(d) Oxalate precipitation :

This method is advantageous for two reasons viz. precipitation can be carried out by ammonium oxalate solution which does not leave any residue after ignition and on account of same crystal structure of metal oxalates precipitation tend to produce mixed crystals, which contain metallic cations in proportions in which they were present in solution.

#### 2.3 PRE-SINTERING :

The purpose pre-sintering is :

1. to decompose carbonates and higher oxides which reduces the evolution of gas in final sintering process.
2. to assist in homogeneizing the material and also reduces the variation in composition of raw material.
3. to reduce the control of shrinkage of material, which occur otherwise during final sintering.

During presintering the raw materials partly react to form final product and amount of reaction depend on reactivity of component and on presintering temperature.<sup>13</sup> The reacted material is then ground to a fine powder before being pressed into required shape.

#### 2.4 SINTERING :

Sintering consist of firing compacted material to high temperatures.

During sintering final microstructure develops. Also densification, grain growth are achieved by sintering process.

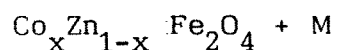
Sintering give rise to variety of microstructure. Sintering reactivity is important for densification.

Before starting sintering, the powder is compacted by dry pressing so that density is high and there is good contact between particles. According to Nabarro<sup>14</sup> and Heirring<sup>15</sup> theory for diffusional microcreep is considered to be the principle mechanism for densification. The surface of pore act as source of vacancies. These vacancies diffuse through bulk of particles to grain boundaries, where they can be discharged. The resulting effect is material transport by migration of individual ions from grain boundaries to pores producing shrinkage. The shrinkage of ferrites during final sintering is entirely dependent on temperature with atmosphere playing minor role.

Sintering process is a sort of solid state reaction, involving heat treatment of compacted material at a temperature upto 1350°C. At this temperature mobility is sufficient to permit the decrease of free energy associated with grain boundaries. The final microstructure with oxygen content and distribution of cation are affected by sintering time, sintering temperature, partial pressure of oxygen or any other sintering atmosphere and cooling rate.

## 2.5 PREPARATION OF FERRITE SAMPLES :

The general formula for our mixed ferrite system is,



where  $x = 0, 0.3, 0.5, 0.7, 1.0$

$M = 0.05$ , At wt. % Al.

and,  $M = 0.05$  mol wt %  $Gd_2O_3$

## 2.6 RAW MATERIALS :

A.R. grade<sup>a</sup> -  $Fe_2O_3$ , ZnO,  $CoCO_3$ , Al,  $Gd_2O_3$

## 2.7 WEIGHING :

The various oxides and carbonates were weighed on a single pan micro balance ( of the least count  $10^{-5}$  gm) in stoichiometric proportions and were mixed thoroughly in acetone medium.

## 2.8

## 2.8 PRESINTERING :

The decomposed mixture was then taken in an agate mortar and thoroughly mixed in A.R. grade acetone. The mixture was allowed to dry and then carefully transferred to a clean dry platinum crucible and presintered in glowbar furnace at  $700^{\circ}\text{C}$  for about 12 hours. The samples were then cooled at  $60^{\circ}\text{C/hr}$  by reducing current. The temperature of furnace was measured by Chromel-Alumel thermocouple along with a digital multimeter. (Plate I).

## 2.9 GRINDING :

Samples were then finely powdered by grinding for two to four hours in an agate mortar using AR grade acetone. The samples were then sieved.

## 2.10 PELLET FORMATION :

The samples were powdered and pellets of about 1.5 cm diameter and mass 1.5 gm were prepared by applying a  $10\text{ton/inch}^2$  pressure for about 5 to 10 minutes in a hydraulic press.

## 2.11 FINAL SINTERING :

The pellets so prepared were taken on a clean platinum foil. The foil along with pellet were kept in glowbar furnace and temperature was slowly raised to  $900^{\circ}\text{C}$ . The samples were kept at  $900^{\circ}\text{C}$  for 24 hours. then the samples were cooled at the rate of  $80^{\circ}\text{C/hr}$  down to room temperature by reducing current. The pellets were finely polished smooth by a fine polish paper. The flow chart of ferrite preparation is depicted in Fig. 2.1.

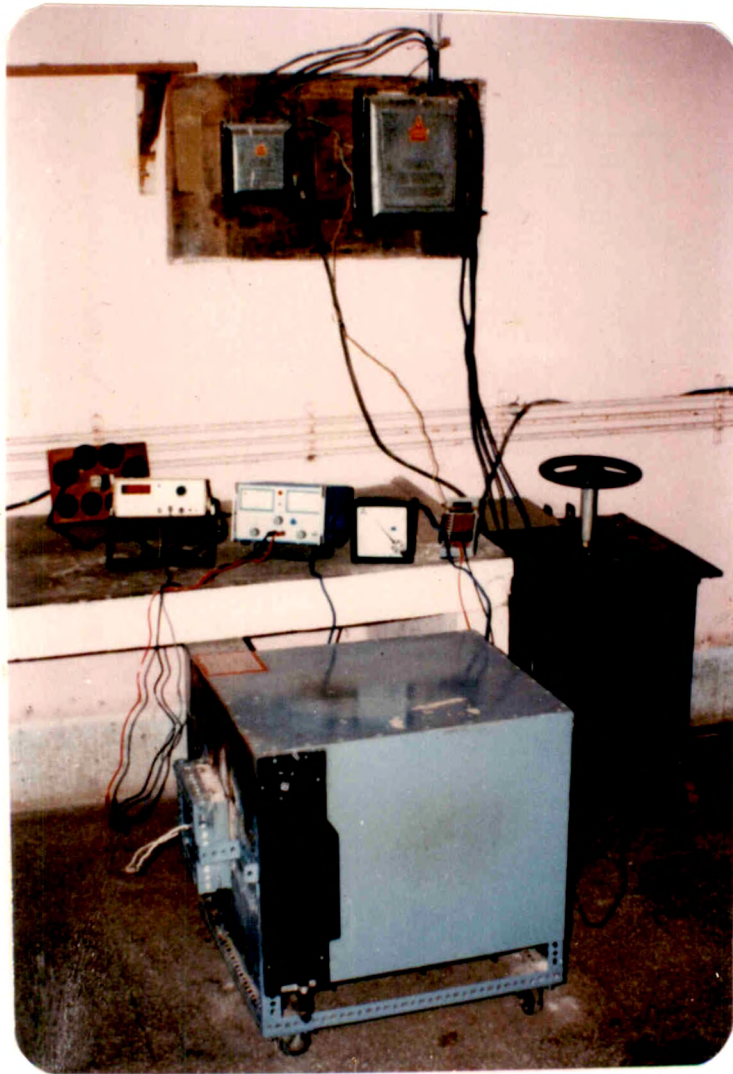


PLATE - I

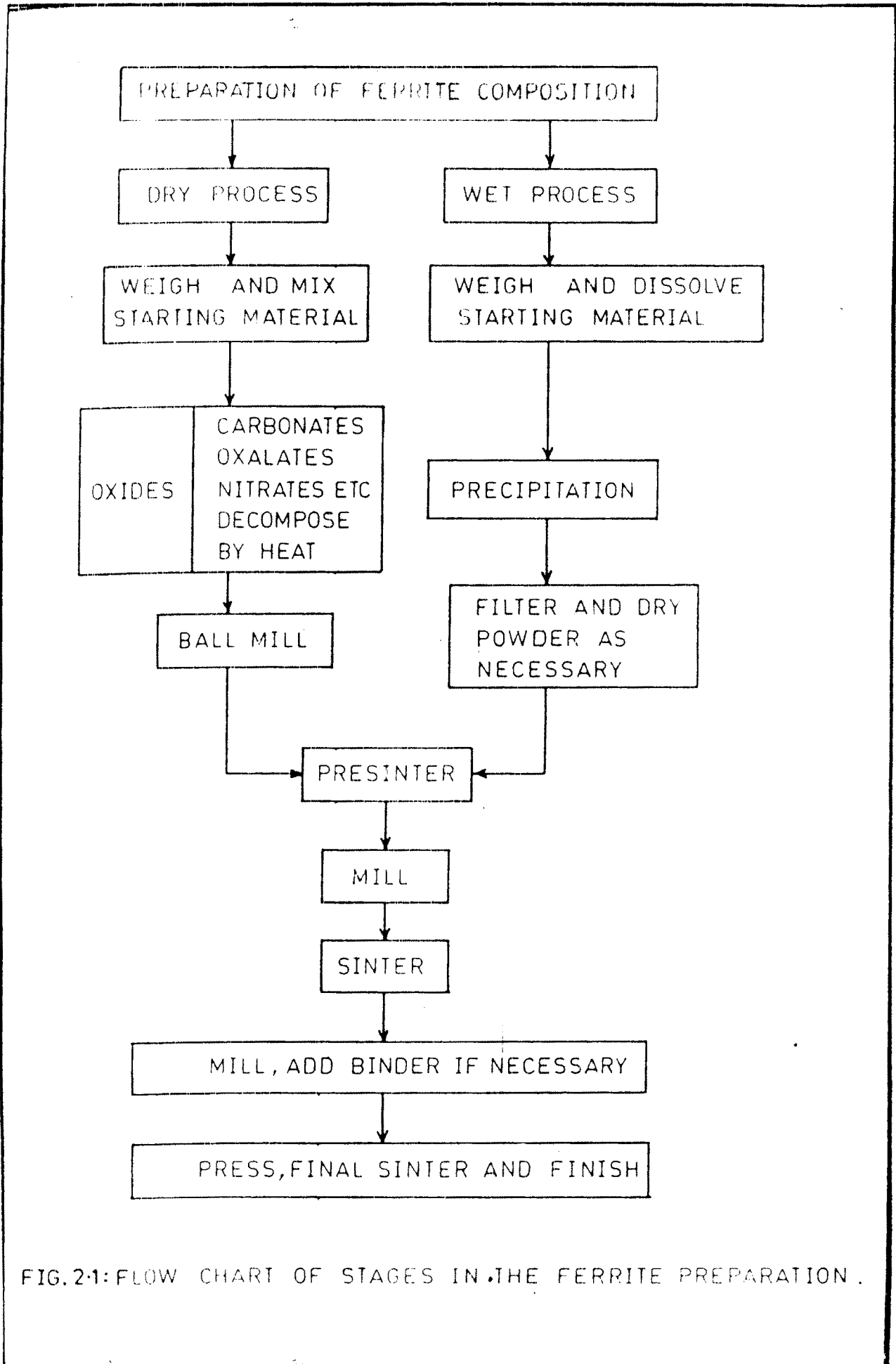


FIG. 2.1: FLOW CHART OF STAGES IN THE FERRITE PREPARATION.

## SECTION B: X-RAY DIFFRACTION STUDIES

### 2.12 INTRODUCTION :

X-ray diffraction (XRD) is well established technique for studying crystal structure in the foresent study XRD pattern are used for confirming formation of ferrite samples, characterisation of crystal structure and to determine lattice constant, the distance between cation and oxygen ion on A site, the distance between cation and on oxygen ion on B site.

### 2.13 CONDITION FOR X-RAY DIFFRACTION :

The regular three dimensional arrangement of unit cell in a crystal can be regarded as a three dimensional diffraction grating According to Bragg<sup>16</sup> it is possible to have diffraction only when wavelength in X-rays are comparable to interplaner distance. Crystal-plane act as partial reflector for X-rays. The Bragg's law can be written as,

$$n\lambda = 2d \sin \theta_{hkl} \quad \dots\dots(2.1)$$

where n - integral number

d- interplanar distance

$\theta_{hkl}$  - Angle through which beam is diffracted.

$$\theta < \sin \theta < 1 \Rightarrow n\lambda < 2d$$

For n =1, diffraction condition for any observable angle 2

$$\lambda < 2d$$

Hence the Bragg's law can be rearranged as

$$\lambda = 2 d/n \sin \theta \quad \dots\dots(2.2)$$

The coefficient  $n$  being unity, reflection of any order can be conveniently considered as first order reflection from Fig. 2.2. In Fig. 2.2a 2nd order [100] reflection is depicted. If there is no real plane midway, between the [100] plane 1st order reflection for adjacent [200] planes (Fig. 2.2b). For cubic crystal<sup>19</sup> the interplaner distance in [hkl] set of planes is given by,

$$1/d^2 = (h^2 + k^2 + l^2)/a^2 \quad \dots\dots(2.3)$$

combining with Bragg's law ,

$$\sin \theta_{hkl} = \lambda^2 / 4a^2 [h^2 + k_2^2 + l^2] \quad \dots\dots(2.4)$$

where 'a' denotes the unit cell size.

The equation (2.4) becomes representative of Bragg's angles for diffraction occurring from the plane (h,k,l) for known values of  $\lambda$ .

#### 2.14 X-RAY DIFFRACTION METHODS :

When X-rays are incident on a crystal lattice, they are diffracted, when Bragg's law is satisfied. The condition for X-ray diffraction can be satisfied either by varying  $\lambda$  or  $\theta$ .

The way in which  $\lambda$  and  $\theta$  are varied projects three different methods.

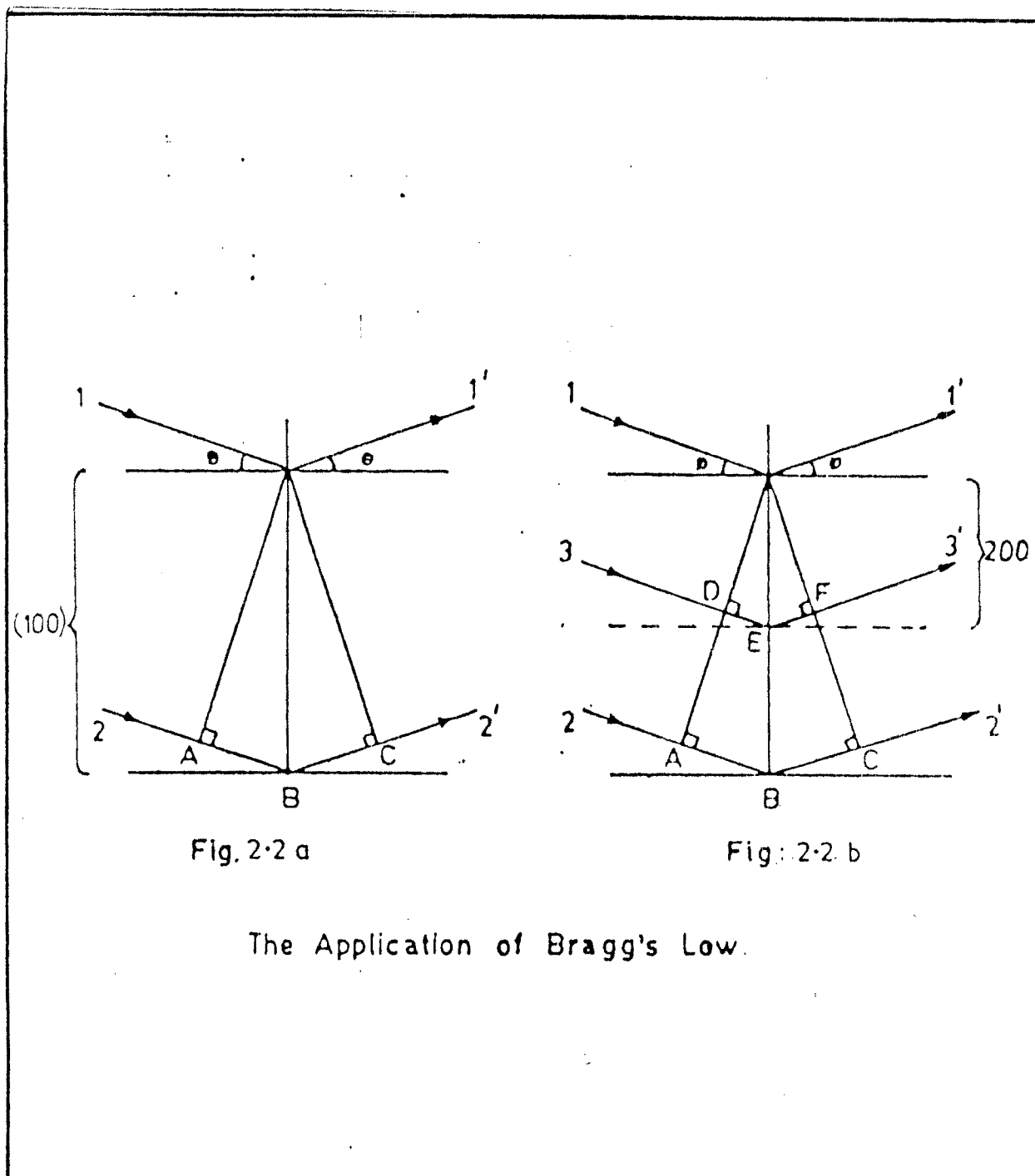


Fig. 2-2

**TABLE 2.1**  
**X-RAY DIFFRACTION METHODS**

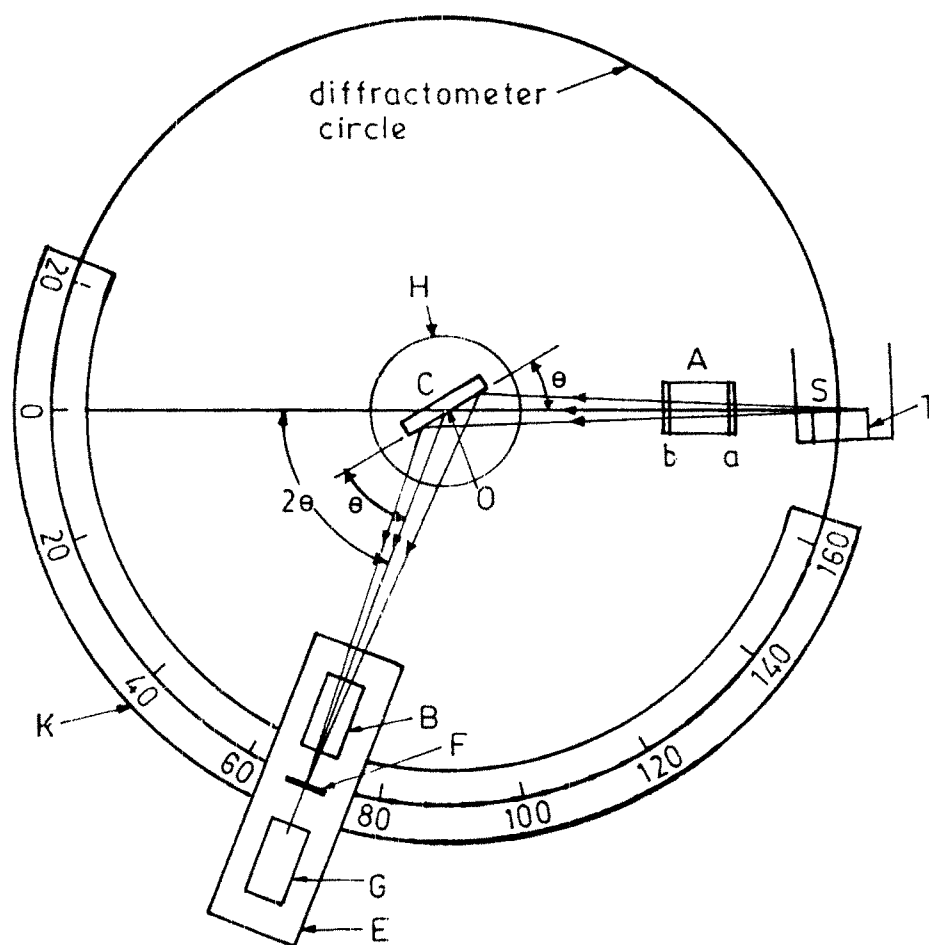
Method	$\lambda$	$\theta$
Laue's method	Variable	Fixed
Rotating Crystal method	Fixed	Variable
Powder method	Fixed	Variable

The powder method was first developed by P. Debye and P. Scherrer<sup>17</sup> and independently by Hull<sup>18</sup>. The powder method is of special importance as well as convenient method, which can be readily applied to polycrystalline materials. It also determines lattice parameter to a greater accuracy and identify phases. Hence the method has been utilised in confirming the ferrite formation as well as for determining lattice parameter and A-O and B-O bond lengths.

#### 2.15 X-RAY DIFFRACTOMETER AND ITS PRINCIPLE :

The film in Debye-Scherrer<sup>17</sup> camera is replaced by a movable counter in an X-ray diffractometer. The principle of diffractometer and its salient features are described in Fig.2.3.

An incident X-ray beam passing through a filter is collimated by slit A. The monochromatic radiation on the specimen kept on



K - Circular scale , G - Counter , E - Carriage ,  
 B-F - Slit , C - Specimen .

Fig.2.3 : X - ray diffractometer schematic .

holder C and thus reflected by crystal planes satisfying Bragg's law. As the crystallites are randomly oriented a reflection at a particular position is due to set of atomic planes satisfying Bragg's condition. As a result convergent beam diffracted by set of parallel planes is produced which come to focus at slit F and then enters counter G. B is a special slit which collimates the diffracted beam. The counter G is connected to count rate meter and output of circuit is fed to a fast automatic recorder which registers a count per second versus  $2\theta$  i.e. gives a graphical record, which is proportional to intensity of diffracted beam. The location of the centroid of peak recorded gives  $2\theta_{hkl}$  for the corresponding reflection.

The carriage 'E' supports the receiving slit and counter. The carriage E is free to rotate about an axis through 'C'. The angular position ' $2\theta$ ' of carriage and hence that of counter G can be noted on graduated circular scale K, through mechanical coupling between E and H. This ensures that complementary angle of incidence and reflection from flat specimen are always equal to each other. The counter receive the focused beam diffracted at glancing angle  $\theta$ . The powder driven counter moves with constant angular velocity about the axis of diffractometer for any desired angular range between  $10^{\circ}$  to  $160^{\circ}$ . Diffractometer has a unique feature that it gives quantitative measure of the intensity of diffracted beam.

#### **2.16 THE DETAILS OF DIFFRACTOMETER :**

In the present work Philips computerised X-ray diffractometer at Shivaji University, Kolhapur was used.

Model- Philips PW 1710 automated powder X-ray diffractometer.

Traget used - Cu with Nickel filter.

Range of  $2\theta$ -  $15^\circ$  to  $85^\circ$

Wavelength-  $1.5418 \text{ \AA}$

Operating voltage - 30 kV

Operating current - 15 ma

## 2.17 INDEXING OF POWDER PATTERN :

The diffractograms of the system :

- i) Undoped  $\text{Co}_x\text{Zn}_{1-x}\text{Fe}_2\text{O}_4$  (Fig.2.4.1 to 2.4.5)
- ii) Doped with 0.05 At wt % Al (Fig.2.5.1 to 2.5.5)
- iii) Doped with 0.05 mol wt %  $\text{Gd}_2\text{O}_3$  (Fig.2.6.1 to 2.6.5)

were obtained with diffractometer. The samples were scanned between ( $2\theta = 15^\circ$ ) to  $2\theta = 85^\circ$ ). The first reflection was observed at about  $2\theta = 30^\circ$ . For cubic lattice the interplanar distance  $d_{hkl}$  lattice parameter  $a$  and the indices  $(h,k,l)$  can be represented by a formula,

$$d_{hkl}^2 = \frac{a^2}{(h^2 + k^2 + l^2)} \quad \dots\dots(2.5)$$

The peaks observed in diffractogram indicate that Bragg's law has been satisfied for those angles.

Bragg law

$$2 d_{hkl} \sin \theta_{hkl} = \lambda \quad (n = 1) \quad \dots\dots(2.6)$$

combining (2.1) and (2.5)

$$2 \left( \frac{a}{\sqrt{h^2 + k^2 + l^2}} \right) \sin \theta_{hkl} = \lambda \quad \dots\dots(2.7)$$

$$\frac{\sin^2 \theta_{hkl}}{h^2 + k^2 + l^2} = \frac{\sin^2 \theta_{hkl}}{S} = \frac{\lambda^2}{4a^2} \quad \dots\dots(2.8)$$

where  $s = h^2 + k^2 + l^2$

The sum S is always an integer and the value of  $\lambda^2/4a^2$  must be constant for any observed peak in the pattern. Thus the set of integers S should be properly selected to yield a constant quotient when divided by one into observed  $\sin^2 \theta$  values. Rearranging the equation (2.8) we get,

$$\sin^2 \theta_{hkl} = \lambda^2 S / 4a^2 \quad \dots\dots(2.9)$$

We find that  $\lambda^2/4a^2$  is the greatest common factor (GCF) in  $\sin^2 \theta$

As the first step GCF was determined from few lines at the lower angles and then all other proper integers were found. Once the integers 'S' were known the indices (h,k,l) of reflecting planes were written down by inspection. If the set of integers satisfying equation (2.8) is not found, then other possible system can be checked.

For tetragonal crystal<sup>19</sup>

$$\sin^2 \theta_{hkl} = \lambda^2 / 4 [ (h^2 + k^2) a^2 + l^2 / c^2 ] \quad \dots\dots(2.10)$$

The lattice parameter 'a' is calculated using (2.5) for (400) plane. For all other planes (h,k,l) values were determined by usual procedure<sup>20</sup>. Also the peak of 100% intensity corresponds to the plane (311) so that lattice parameter in this case is calculated using the equation (2.5) and the remaining peaks were indexed.

## 2.18 RESULTS AND DISCUSSION :

X-ray diffractograms of the series  $\text{Co}_x\text{Zn}_{1-x}\text{Fe}_2\text{O}_4$  ( $x=0, 0.3, 0.5, 0.7, 1.0$ ) undoped and (i) doped with 0.05, At wt % Al and (ii) doped with 0.05 mol %  $\text{Gd}_2\text{O}_3$  were obtained. The diffractograms maxima were indexed by method explained above, were checked and tallied with those for spinel structure. The allowed reflections indicate the formation of ferrite phase and confirm the spinel structure. The allowed reflections in X-ray diffraction pattern for spinel structure are as follows :

Cubic (111), (220), (311), (222), (400) (422) (333), (511) (440)

Tetragonal (111), (202), (220), (113), (311), (222), (004), (400), (422), (511), (404), (440).

It is observed that for all the samples, the observed and calculated 'd' values agree well.

This close agreement between observed and calculated 'd' value as reported on diffractogram is a clear indication of the fact that ferrites are fully formed with spinel structure.

DIFFRACTOGRAM OF UNDOPED ZnFe<sub>2</sub>O<sub>4</sub>

(311)

(hkl)	(111)	(220)	(311)	(400)	(333/ 521)	(440)
d observed A <sup>o</sup>	4.868	2.981	2.543	2.108	1.721	1.491
d calculated A <sup>o</sup>	4.851	2.983	2.543	2.109	1.723	1.492

(440)

(333/521)

(422)

(400)

(220)

(111)



FIG. 2.4.1

DNB-1. SM

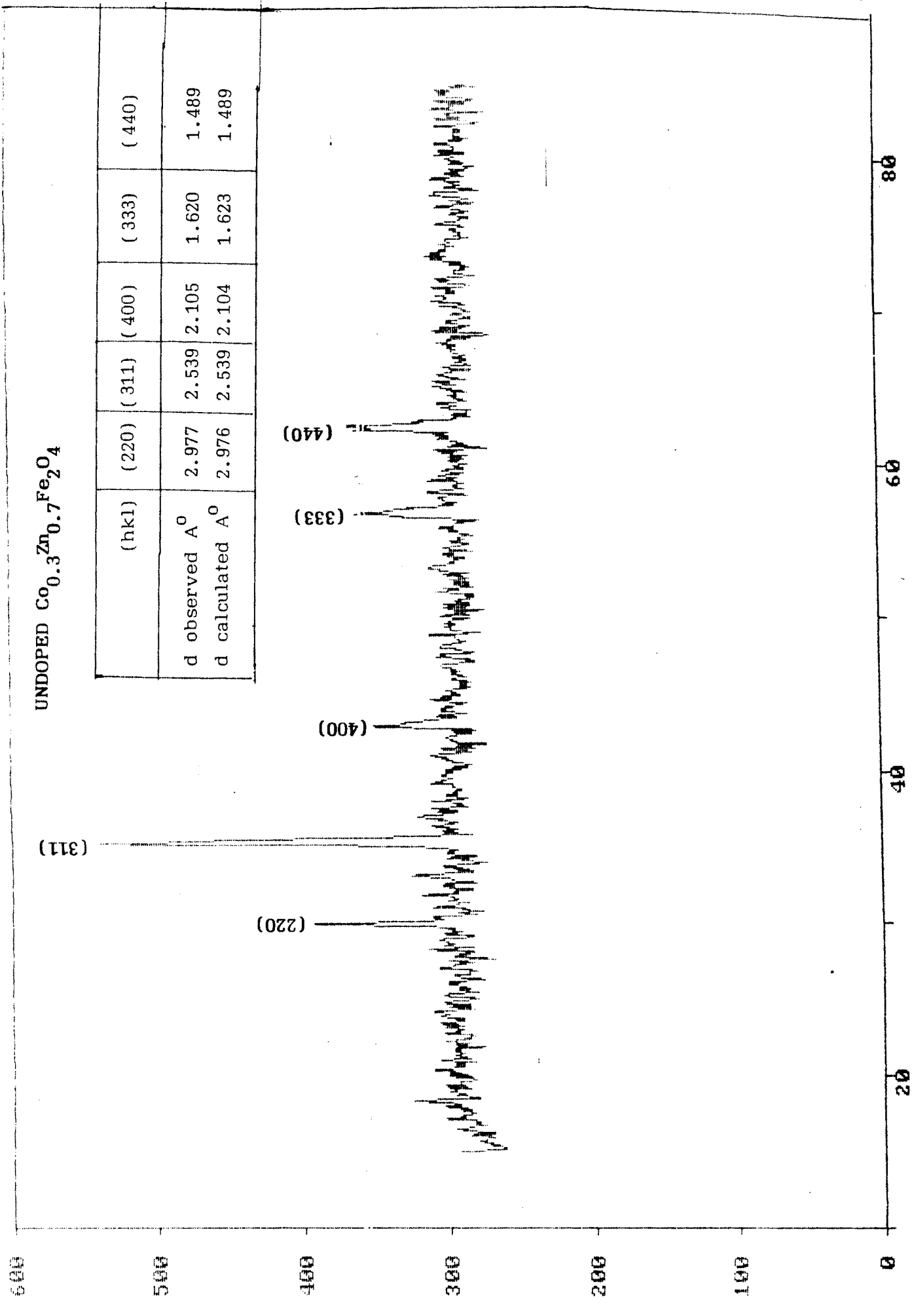


FIG. 2.4.2

DIFFRACTOGRAM OF UNDOPED  $\text{Co}_{0.5}\text{Zn}_{0.5}\text{Fe}_2\text{O}_4$

hkl	220	311	400	333	440
d observed $\text{\AA}$	2.972	2.534	2.102	1.618	1.486
d calculated $\text{\AA}$	2.971	2.534	2.102	1.619	1.487

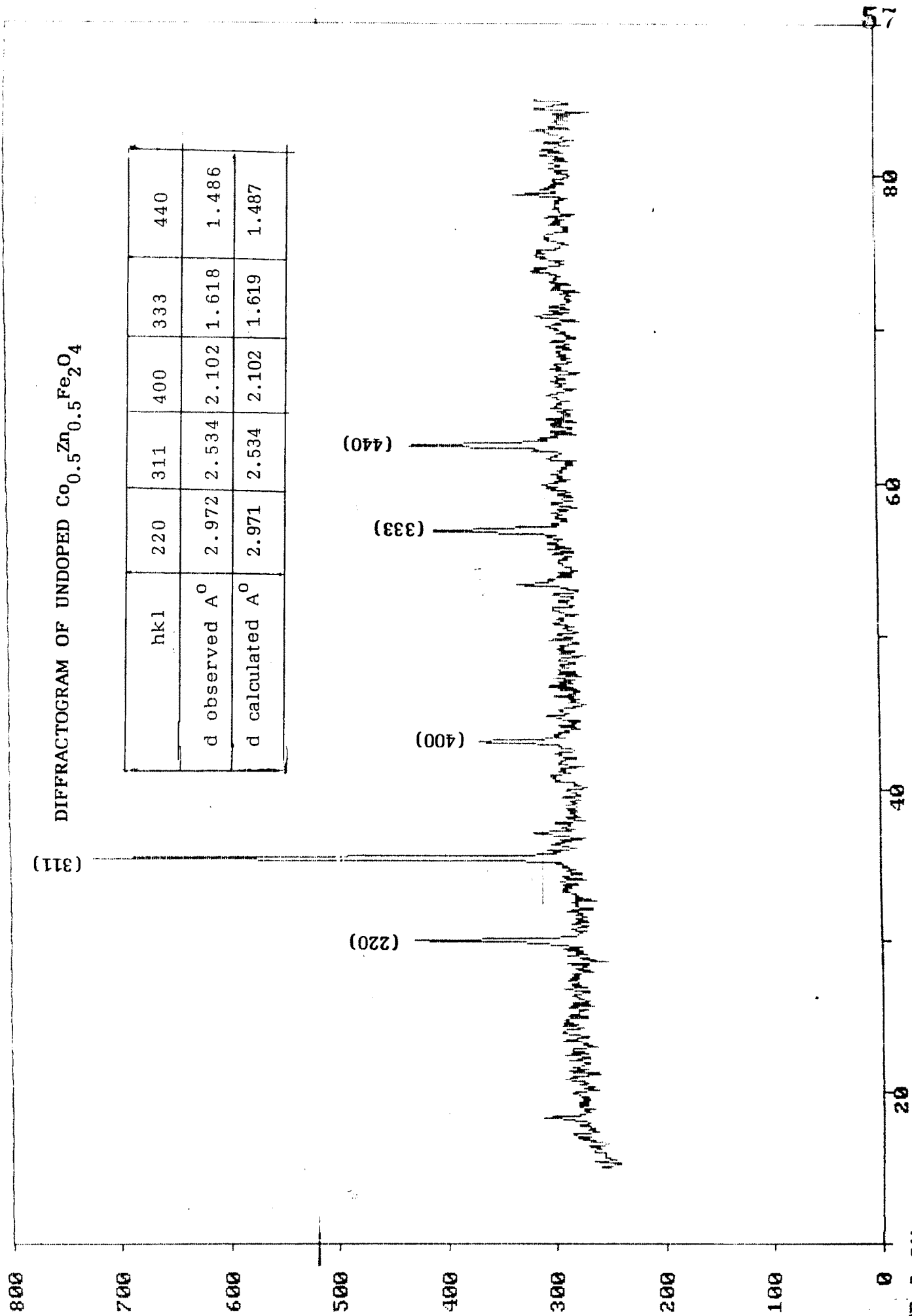


FIG.2.4.3

DIFFRACTOGRAM OF UNDOPED  $\text{Co}_{0.7}\text{Zn}_{0.3}\text{Fe}_2\text{O}_4$

hkl	220	311	400	333	440
d observed $\text{Å}^\circ$	2.968	2.531	2.099	1.616	1.484
d calculated $\text{Å}^\circ$	2.968	2.531	2.099	1.616	1.486

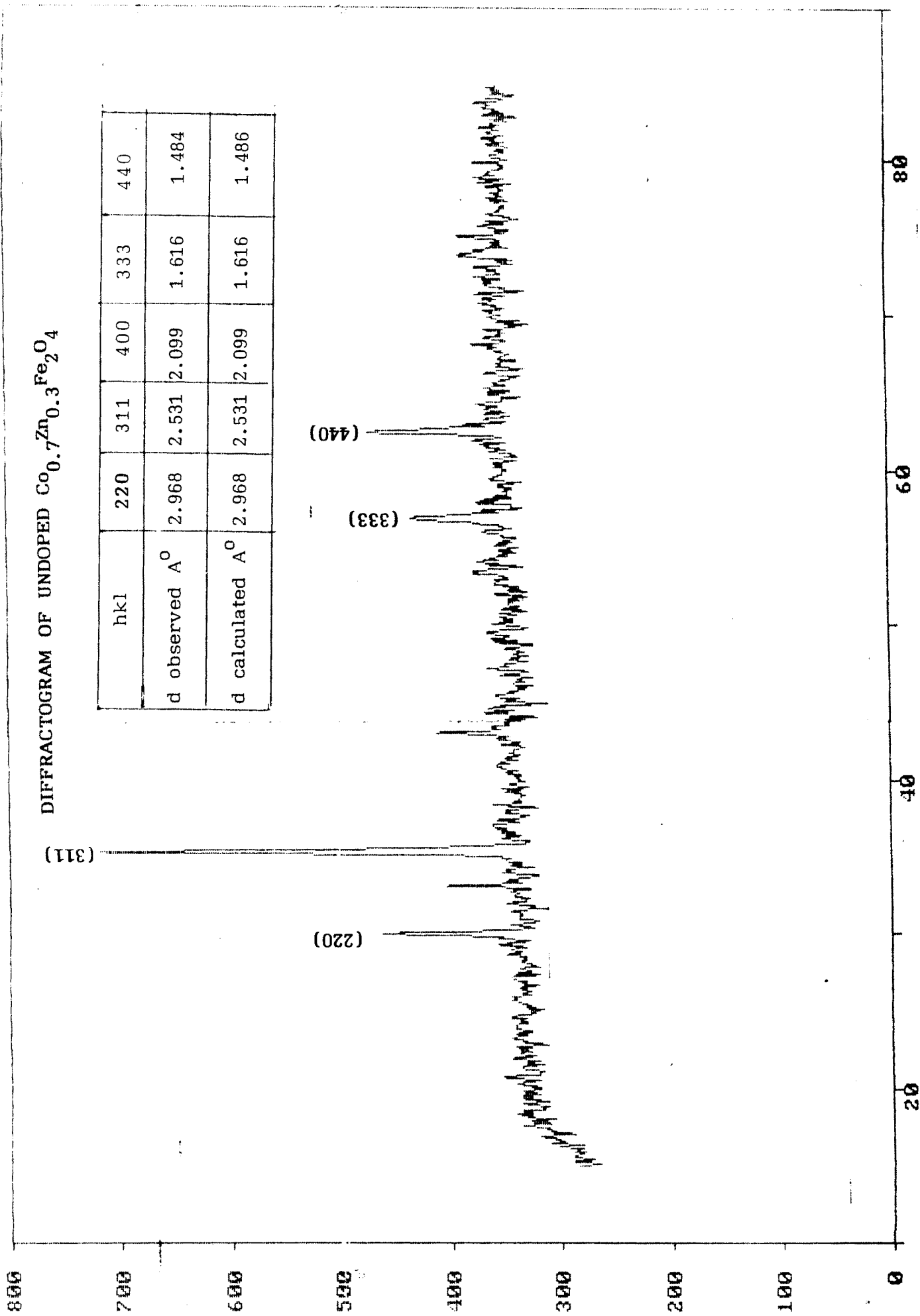
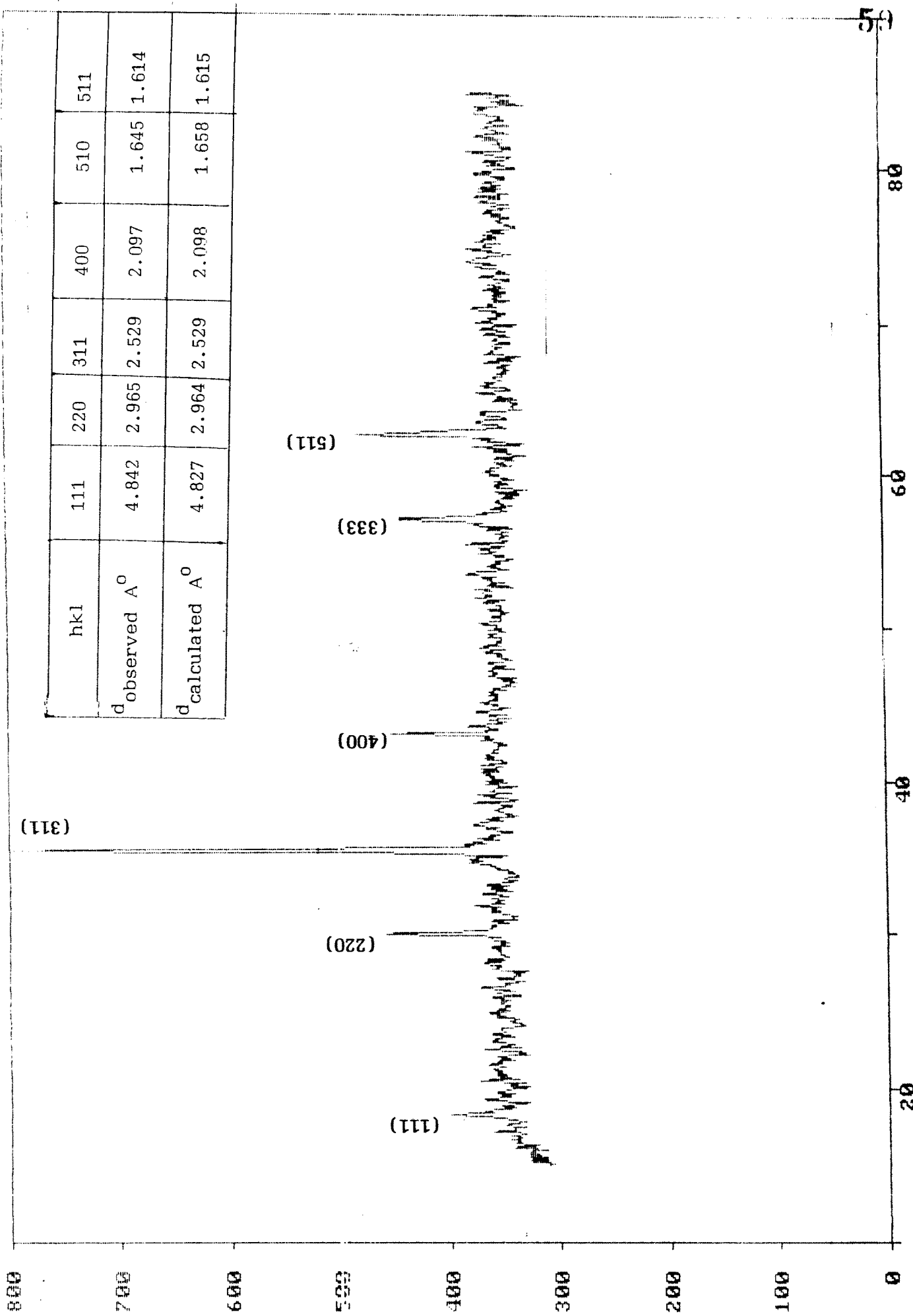


FIG. 2.4.4

DIFFRACTOGRAM OF UNDOPED  $\text{CoFe}_2\text{O}_4$



hkl	111	220	311	400	510	511
d <sup>o</sup> <sub>observed</sub>	4.842	2.965	2.529	2.097	1.645	1.614
d <sup>o</sup> <sub>calculated</sub>	4.827	2.964	2.529	2.098	1.658	1.615

1000

900

800

700

600

500

400

300

200

100

0

DIFFRACTOGRAM OF  $ZnFe_2O_4$  DOPED WITH 0.05 At. Wt. % Al.

hkl	220	311	400	422	333	440
$d_{\text{observed}}$	2.981	2.542	2.107	1.721	1.623	1.491
$d_{\text{calculated } A^0}$	2.980	2.542	2.107	1.723	1.624	1.491

(311)

(220)

(400)

(422)

(333)

(440)

80

60

40

20

DIFFRACTOGRAM OF  $\text{Co}_{0.3}\text{Zn}_{0.7}\text{Fe}_2\text{O}_4$  DOPED WITH 0.05 At. wt. % Al.

hkl	220	311	400	333	440
$d_{\text{observed}} \text{ \AA}$	2.981	2.542	2.093	1.622	1.490
$d_{\text{calculated}} \text{ \AA}$	2.984	2.542	2.104	1.623	1.491

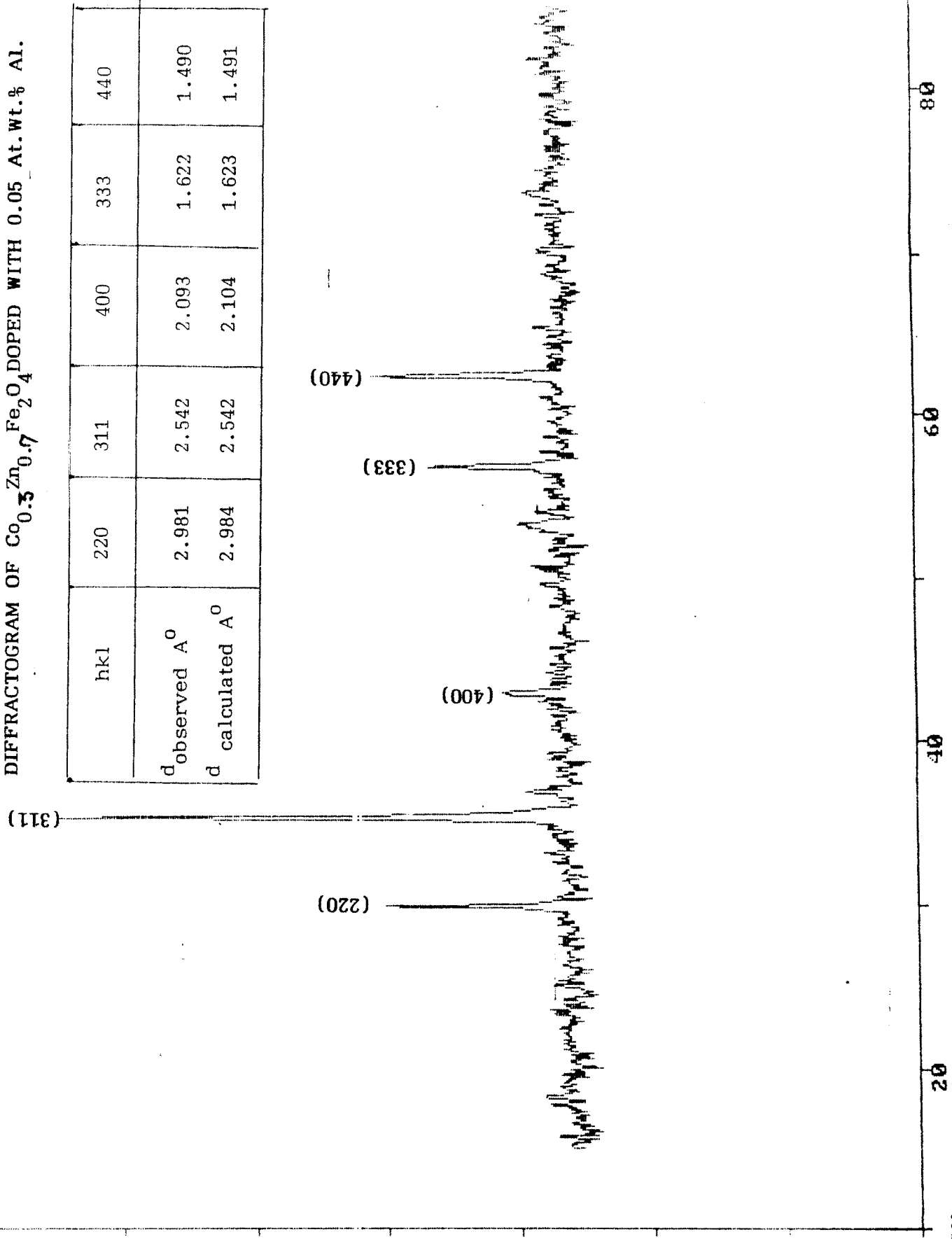


FIG. 2.5.2

800

700

600

500

400

300

200

100

0

COUNT

(311)

(220)

(400)

(333)

(440)

DIFFRACTOGRAM OF  $\text{Co}_{0.5}\text{Zn}_{0.5}\text{FeO}_{2.4}$  DOPED WITH 0.05 At.%. Al

hkl	220	311	400	333	440
d observed $\text{\AA}^{\circ}$	2.974	2.536	2.103	1.619	1.487
d calculated $\text{\AA}^{\circ}$	2.974	2.536	2.102	1.619	1.488

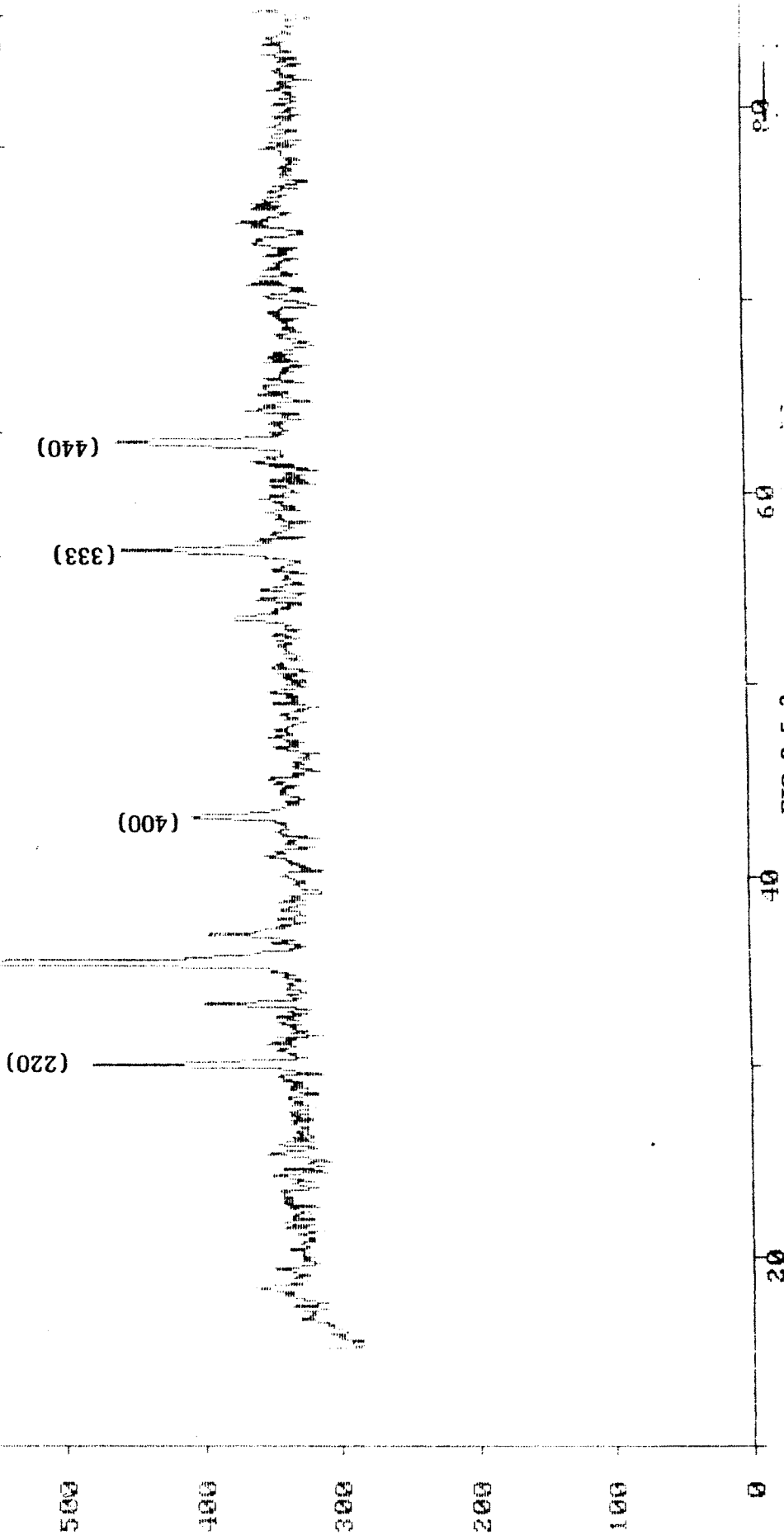


FIG.2.5.3

900

800

700

600

500

400

300

200

100

0

DIFFRACTOGRAM OF  $\text{Co}_{0.7}\text{Zn}_{0.3}\text{Fe}_2\text{O}_4$  DOPED WITH 0.05 AT. WT. % AL.

hkl	220	311	400	333	440
d	2.972	2.535	2.102	1.618	1.486
d	2.970	2.535	2.100	1.618	1.486

(311)

(220)

(400)

(333)

(440)

20

40

60

80

DNB-9.SM

FIG. 2.5.4

63

DIFFRACTOGRAM OF  $\text{CoFe}_2\text{O}_4$  DOPED WITH 0.05 AT. WT. % AL.

hkl	220	311	400	333/511	440
d observed $\text{\AA}^\circ$	2.963	2.527	2.095	1.612	1.481
d calculated $\text{\AA}^\circ$	2.963	2.527	2.092	1.613	1.482

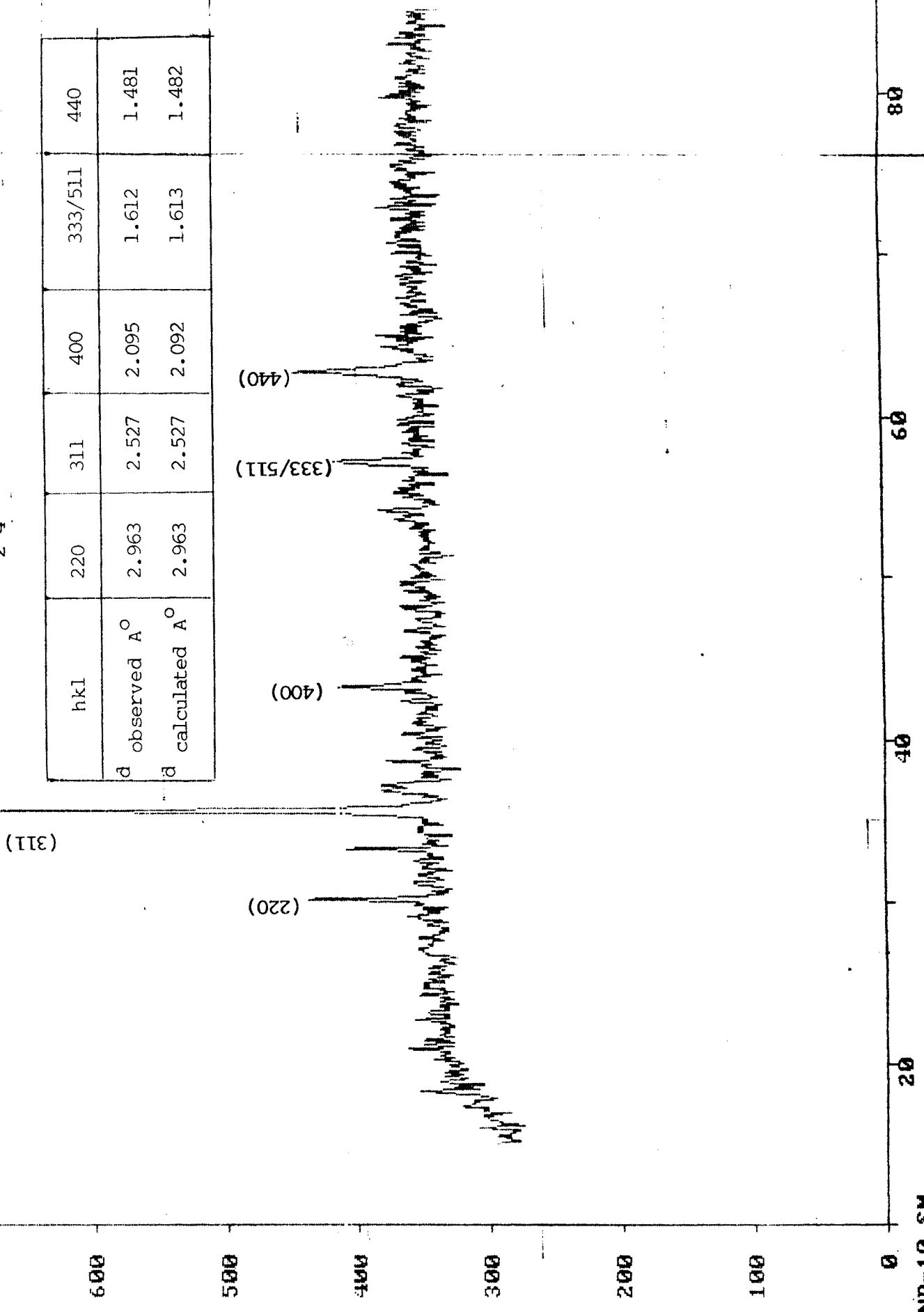


FIG. 2.5.5

DNB-10. SM

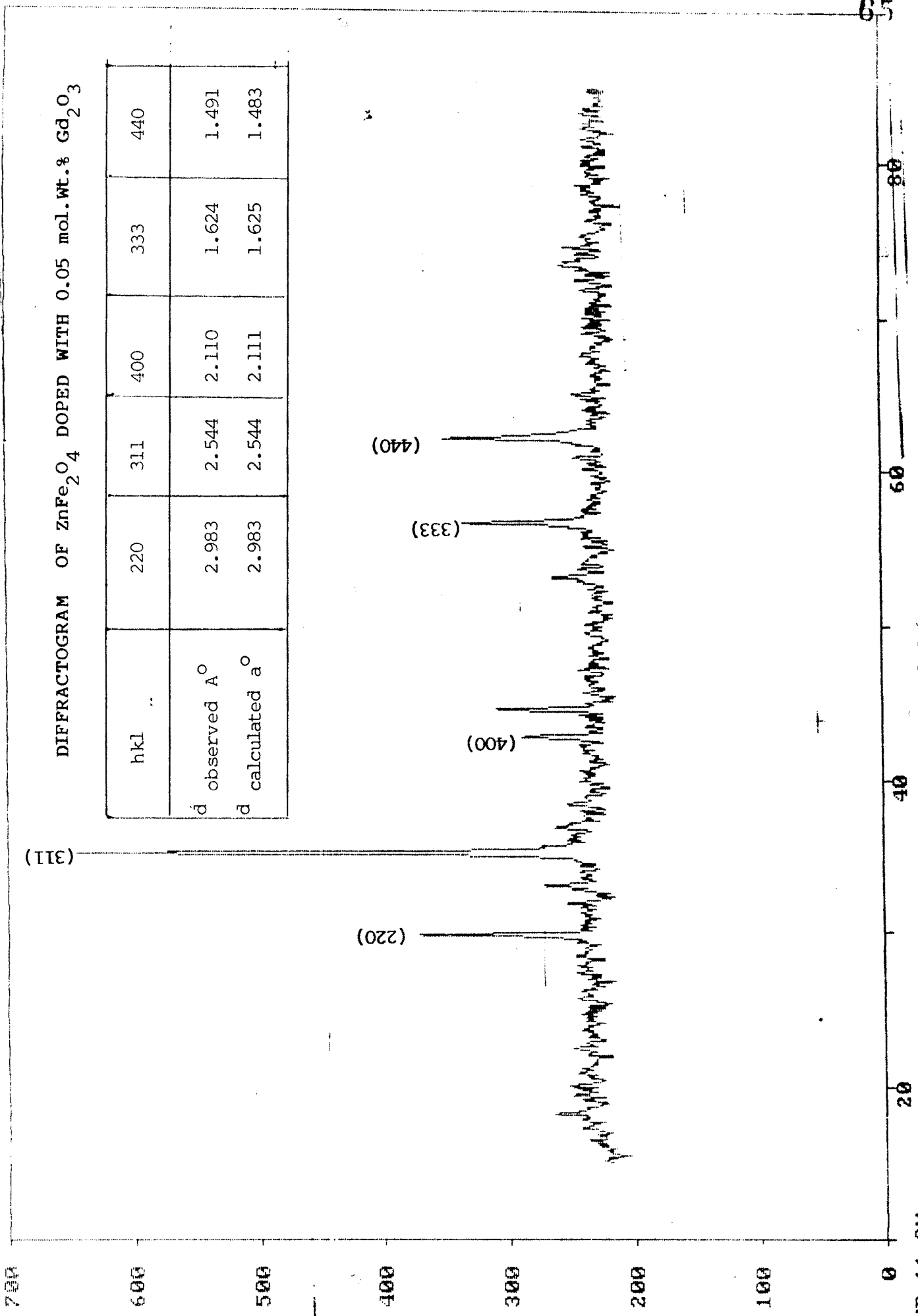


FIG. 2.6.1

8400

7000

6000

5000

4000

3000

2000

1000

0

(311)

DIFFRACTOGRAM OF  $\text{Co}_{0.3}\text{Zn}_{0.7}\text{FeO}_2$  DOPED WITH 0.05 mol.wt.%  $\text{Gd}_2\text{O}_3$ 

hkl	220	311	400	333	440
d observed $\text{\AA}^\circ$	2.974	2.536	2.103	1.619	1.487
d calculated $\text{\AA}^\circ$	2.969	2.536	2.103	1.621	1.489

(220)

(440)

(333)

(400)

20

40

60

80

100

700

600

500

400

300

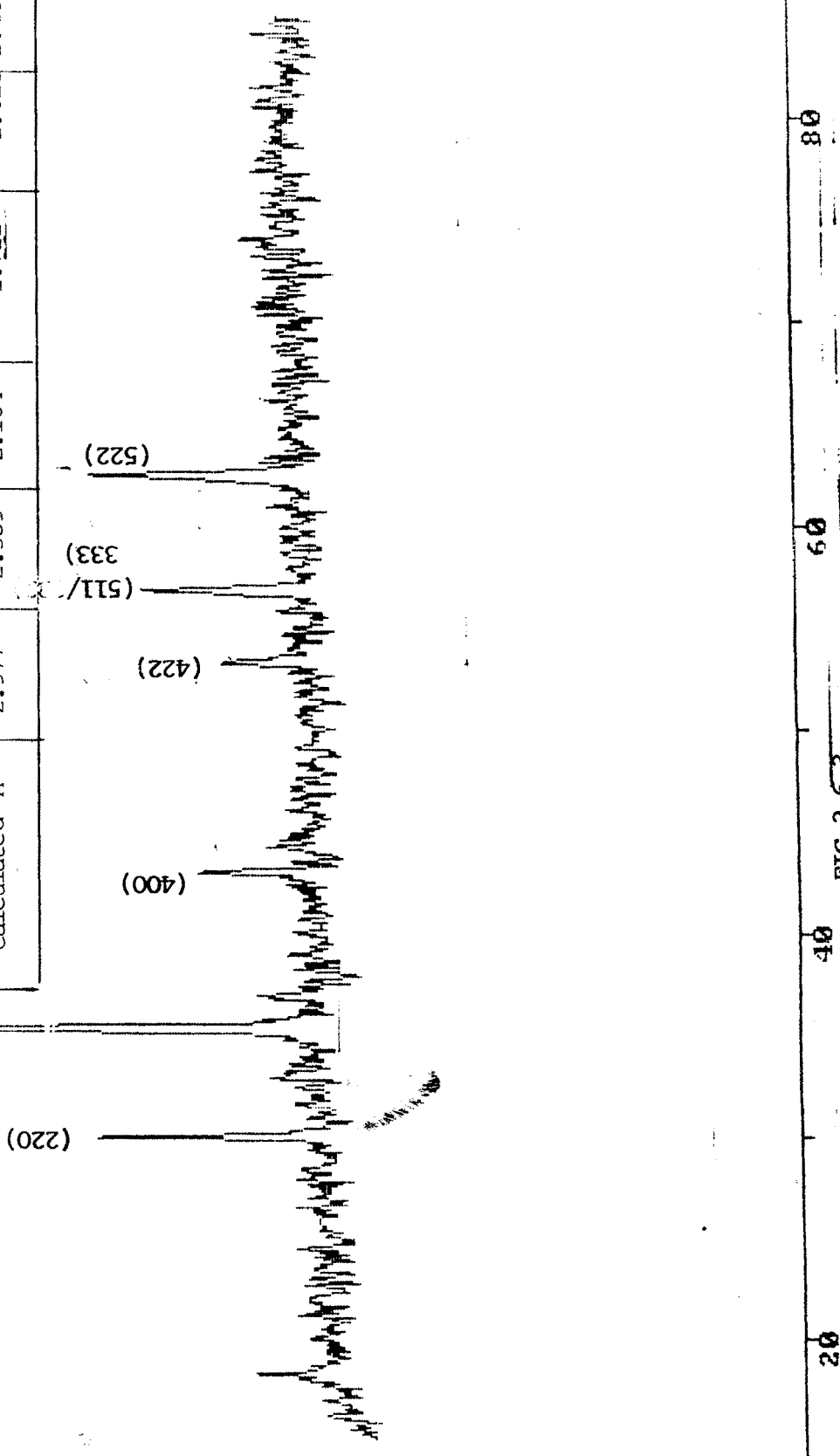
200

100

0

(311) DIFFRACTOGRAM OF  $\text{Co}_{0.5}\text{Zn}_{0.5}\text{Fe}_2\text{O}_4$  DOPED WITH 0.05 mol. wt. %  $\text{Gd}_2\text{O}_3$

hkl	220	311	400	422	511 / 333	522
p observed $\lambda^\circ$	2.977	2.539	2.105	1.719	1.620	1.466
p calculated $\lambda^\circ$	2.977	2.539	2.104	1.712	1.618	1.487



600

500

400

300

200

100

0

20

40

60

80

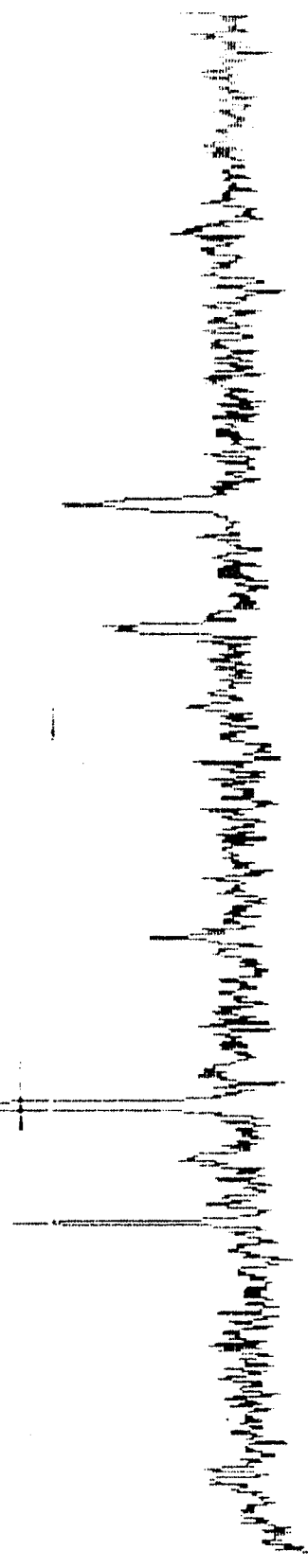
57

DNB-14. SM

FIG. 2.6.4

DIFFRACTOGRAM OF  $\text{Co}_{0.7}\text{Zn}_{0.3}\text{Fe}_2\text{O}_4$  DOPED WITH 0.05 MOL. WT. %  $\text{Gd}_2\text{O}_3$

hkl	220	311	400	333	440
d	2.966	2.529	2.097	1.614	1.482
d	2.965	2.529	2.104	1.616	1.485



DIFFRACTOGRAM OF  $\text{CoFe}_2\text{O}_4$  DOPED WITH 0.05 Mol. Wt. %  $\text{Gd}_2\text{O}_3$

(311)

hkl	220	311	400	440
d observed $\text{A}^\circ$	2.964	2.528	2.096	1.482
d calculated $\text{A}^\circ$	2.961	2.528	2.096	1.482

(220)

(400)

(440)

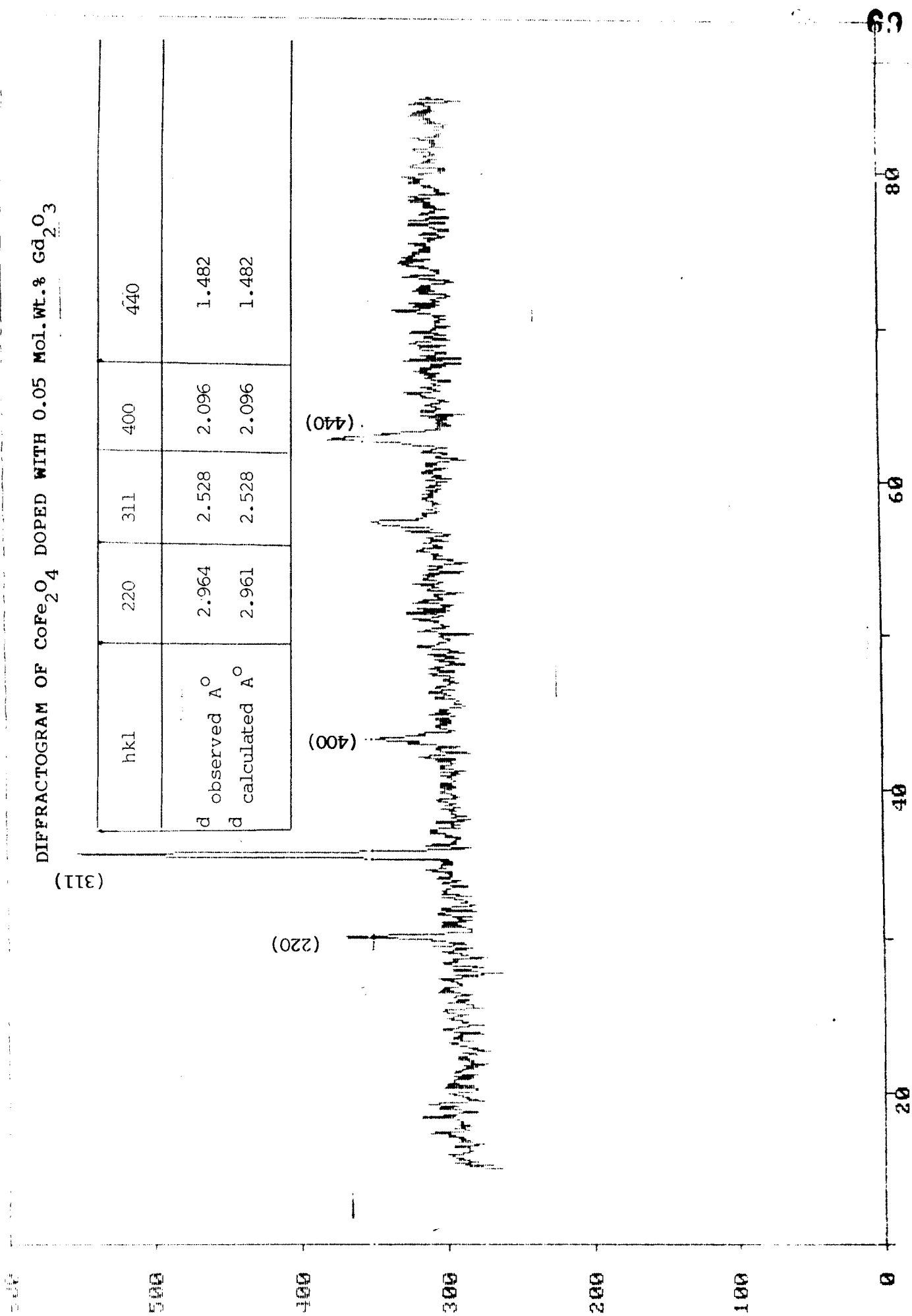


TABLE 2.2  
THE VALUES OF LATTICE CONSTANTS

Composition	LATTICE CONSTANT IN Å <sup>0</sup>		
	Without doping	with doping 0.05 At.Wt.% of Aluminium	with doping 0.05 mol.Wt.% of Gd <sub>2</sub> O <sub>3</sub>
Co <sub>0</sub> ZnFe <sub>4</sub> O <sub>4</sub>	8.433	8.432	8.439
Co <sub>0.3</sub> Zn <sub>0.7</sub> Fe <sub>2</sub> O <sub>4</sub>	8.421	8.430	8.432
Co <sub>0.5</sub> Zn <sub>0.5</sub> Fe <sub>2</sub> O <sub>4</sub>	8.405	8.412	8.420
Co <sub>0.7</sub> Zn <sub>0.3</sub> Fe <sub>2</sub> O <sub>4</sub>	8.395	8.409	8.389
Co <sub>1.0</sub> Zn <sub>0.0</sub> Fe <sub>2</sub> O <sub>4</sub>	8.389	8.380	8.384

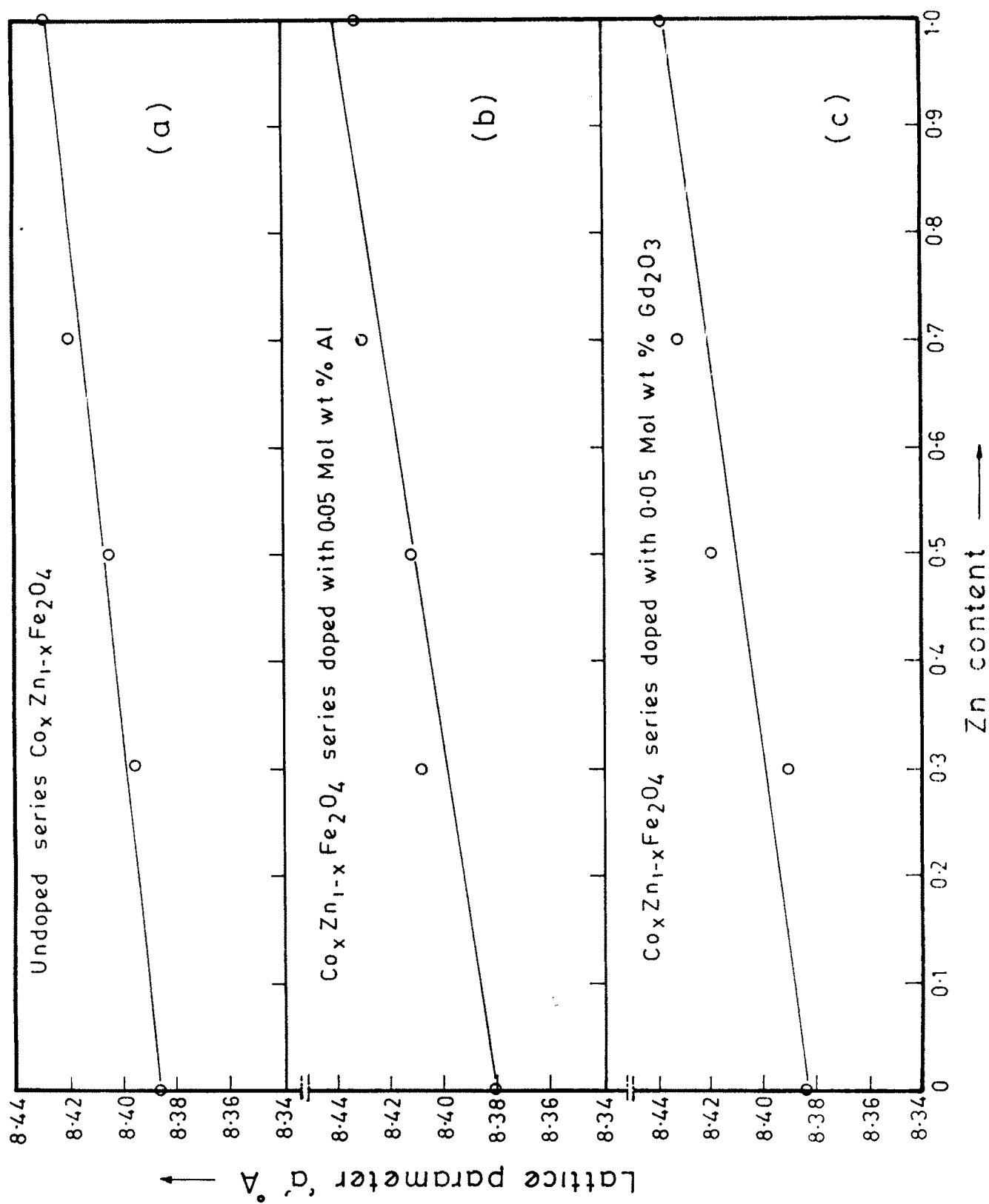


Fig. 2.7

From the table 2.2 it is observed that the lattice constant increases with increase of zinc concentration. Josyulu and Sobhanadri<sup>34</sup> have also observed the similar behaviour for Co-Zn ferrite system. The slight variation in the lattice constant for the present series with that of reported values may be due to preparation conditions and heat treatment. The linear relationship between two (i.e. Cobalt ferrite and Zinc ferrite) indicates the applicability of Vegard's law in this case and hence completion of solid state reaction. The variation in lattice constant may be explained on the basis of differences in ionic radii of the elements. considering the ionic radii of Cobalt ( $0.78 \text{ \AA}$ ) and Zinc ( $0.83 \text{ \AA}$ ), the ionic radii and hence ionic volume of Zinc is larger than that of Cobalt and hence the increase of lattice constant with increase of Zinc concentration. In table 2.3 ionic radii of the cation involved are given.<sup>21</sup>

**TABLE 2.3**  
**IONIC RADII**

Ion	Co <sup>3+</sup>	Zn <sup>2+</sup>	Fe <sup>3+</sup>	Al <sup>3+</sup>	Gd <sup>3+</sup>
Ionic radii $\text{ \AA}$	0.78	0.83	0.65	0.53	0.94

The Aluminium doped and Gadolinium doped series  $\text{Co}_x\text{Zn}_{1-x}\text{Fe}_2\text{O}_4$  show a similar behaviour. The slight variation of lattice constant in case of undoped and doped series may be due to variation in cation distribution or modification in the lattice. (Fig.2.7)

The bond lengths were computed by using formula,

$$R_A = a\sqrt{3} (\delta + 1/8) \quad \dots\dots(2.11)$$

and

$$R_B = a\sqrt{3\delta^2 - 1/2\delta + 1/16}$$

where  $\delta = u - 0.375$  and  $u$  has taken the average value of end ferrites.

$R_A$  and  $R_B$  increase with increase of Zinc concentration (Table 2.4)

Levine's<sup>22</sup> recent work on bond susceptibilities shows that decrease in bond length correspond to increase in covalent character of spinel from Table 2.4. It is seen that for mixed Co-Zn ferrite system A-O and B-O distance go on increasing with increase of zinc concentration. Therefore, Cobalt ferrite is more covalent than Zinc ferrite. Hence it can be concluded that bond distances exhibit sensitive dependence on covalency and composition.

X-ray density  $\rho_x$  value reported in Table 2.5.

TABLE 2.4  
BOND LENGTHS

Composition	BOND LENGTH IN Å <sup>0</sup>					
	Without doping		With doping 0.05 At. wt.% of Aluminium		with doping of 0.05 mol.Wt.% of Gd <sub>2</sub> O <sub>3</sub>	
	R <sub>A</sub>	R <sub>B</sub>	R <sub>A</sub>	R <sub>B</sub>	R <sub>A</sub>	R <sub>B</sub>
Co <sub>0.0</sub> Zn <sub>1.0</sub> Fe <sub>2</sub> O <sub>4</sub>	1.97	2.26	1.97	2.20	1.92	2.06
Co <sub>0.3</sub> Zn <sub>0.7</sub> Fe <sub>2</sub> O <sub>4</sub>	1.95	2.23	1.95	2.04	1.95	2.055
Co <sub>0.5</sub> Zn <sub>0.5</sub> Fe <sub>2</sub> O <sub>4</sub>	1.94	2.24	1.94	2.04	1.94	2.04
Co <sub>0.7</sub> Zn <sub>0.3</sub> Fe <sub>2</sub> O <sub>4</sub>	1.92	2.16	1.93	2.04	1.92	2.04
Co <sub>1.0</sub> Zn <sub>0.0</sub> Fe <sub>2</sub> O <sub>4</sub>	1.990	2.05	1.90	2.04	1.90	2.03

TABLE 2.5

## X-RAY DENSITIES

Composition	X-RAY DENSITY gram/cc		
	without doping	With doping 0.05 At.Wt.% of Aluminium	with doping 0.05 mol.Wt.% of Gd <sub>2</sub> O <sub>3</sub>
Co <sub>0</sub> ZnFe <sub>2</sub> O <sub>4</sub>	5.342	5.345	5.331
Co <sub>0.3</sub> Zn <sub>0.7</sub> Fe <sub>2</sub> O <sub>4</sub>	5.321	5.304	5.339
Co <sub>0.5</sub> Zn <sub>0.5</sub> Fe <sub>2</sub> O <sub>4</sub>	5.323	5.281	5.260
Co <sub>0.7</sub> Zn <sub>0.7</sub> Fe <sub>2</sub> O <sub>4</sub>	5.314	5.316	5.353
Co <sub>1.0</sub> Zn <sub>0.0</sub> Fe <sub>2</sub> O <sub>4</sub>	5.284	5.298	5.290

## SECTION C : INFRARED STUDIES :

FAR INFRARED SPECTRA OF  $\text{CO}_x\text{Zn}_{1-x}\text{Fe}_2\text{O}_4$  WITHOUT AND WITH DOPING

## 2.19 INTRODUCTION :

Infrared spectra is an important tool to describe various ordering parameters. The optical spectra of ferrite gives information about various vibrational modes in the presence or absence of  $\text{Fe}^{2+}$  ions, whereas, the vibrational, electronic and magnetic dipole spectra give information about position and valency of ions. It provides unmistakable "Finger-prints", hence is widely popular amongst Physicist and chemists.

Waldron<sup>23</sup> had reported infrared spectra of several simple ferrites with general formula  $\text{MeFe}_2\text{O}_4$ . He had reported four optical bands corresponding to four infrared active fundamental modes ( $T_1, u$ ), in vibration spectra of normal and inverse spinel. He assigned the broad and a symmetric high frequency band  $\nu_1$  to tetrahedral group complexes and low frequency band  $\nu_2$  to octahedral complexes. The broad and asymmetric high frequency band, depend on grain size and condition of preparation. They give rise to distinct shoulder or even splitting of bands. The other two bands at low frequencies are independent of method of preparation and condition of preparation.

Tarte<sup>24</sup> has suggested that nature of these vibrations mainly, depend on the identity of transition metal ion in octahedral site and to a smaller extent on ions situated in tetrahedral voids of spinel.

Tarte<sup>24</sup>, Halfer<sup>25</sup> and Preudhomme<sup>26</sup> and other<sup>27,28</sup> studied infrared spectra of some normal and inverse spinel ferrites. Preudhomme distinguished three applications in connection with application of I.R. spectroscopy to crystal chemistry of spinel viz.

- i) the determination of coordination of cations in the spinel structure.
- ii) the study of cation disordering.
- iii) the study of deformation of the cubic spinel structure.

Barbers<sup>29,30,31</sup> observed splitting of bonds in cubic and tetragonal manganese ferrite ( $Mn_xFe_{3-x}Fe_2O_4$ ) in the range  $700\text{ cm}^{-1}$  with  $X > 1$ . Most of work done by him to understand ionic ordering of  $Ti^{4+}$  containing spinels. He concluded that there are local tetragonal distortion which has its origin in John-Teller effect of octahedral  $Mn^{3+}$  ions. Klerk<sup>32</sup> studied I.R. spectra of  $MnFe_2O_4$  with degree of inversion of Mn about 0.05 and 0.2. He concluded that absorption band observed at  $335\text{ cm}^{-1}$  has to be third fundamental I.R. active mode. V.R.K.Murthy et al<sup>33</sup> have studied the I.R. absorption in Ni-Zn ferrites. The variation is similar to that observed by introducing foreign atoms in the spinel.

## 2.20 EXPERIMENTAL TECHNIQUE :

The far infrared spectra of Cobalt, Cobalt-Zinc, zinc ferrites undoped and doped were obtained by KBr pellet method. The ferrite powder were dispersed in KBr and pressed to get a clear disc

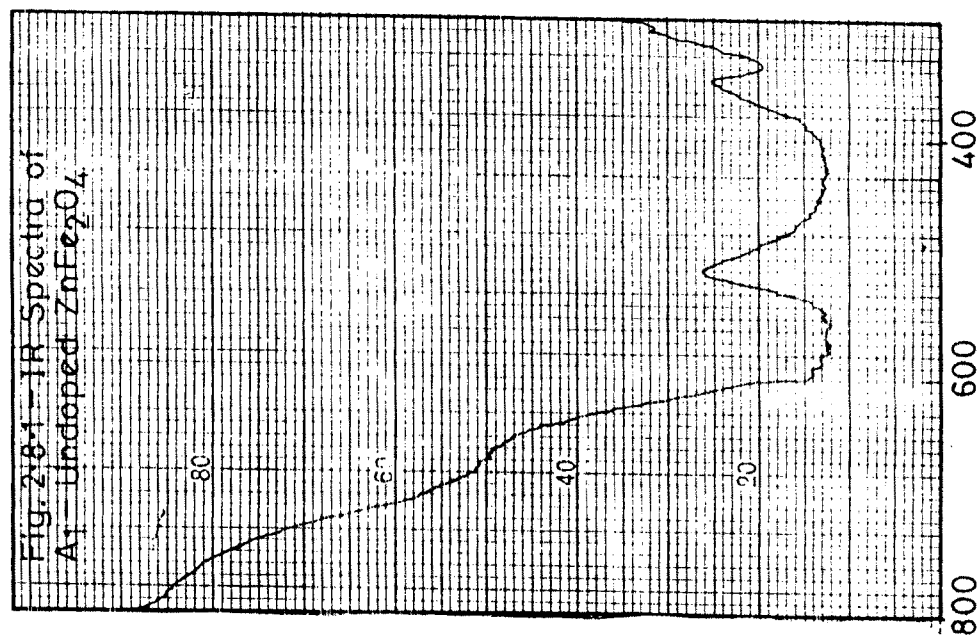
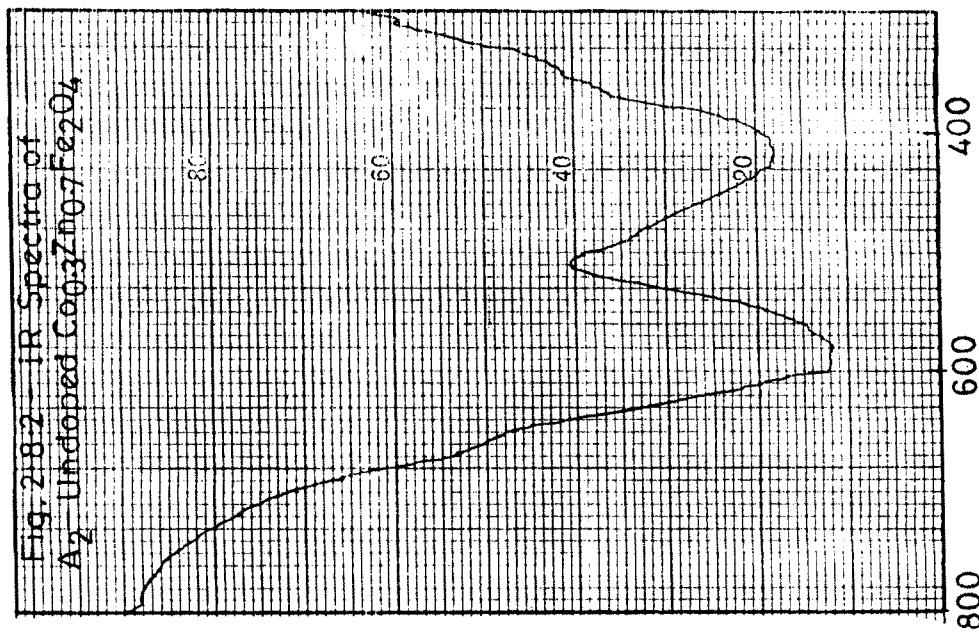
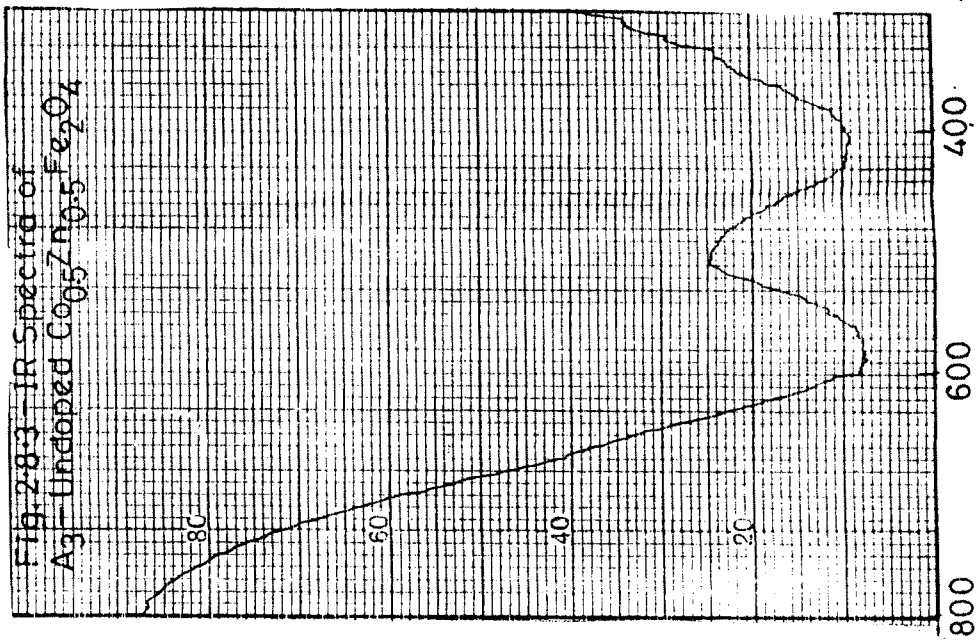
Model-Perkin Elmer at Shivaji University, Kolhapur.

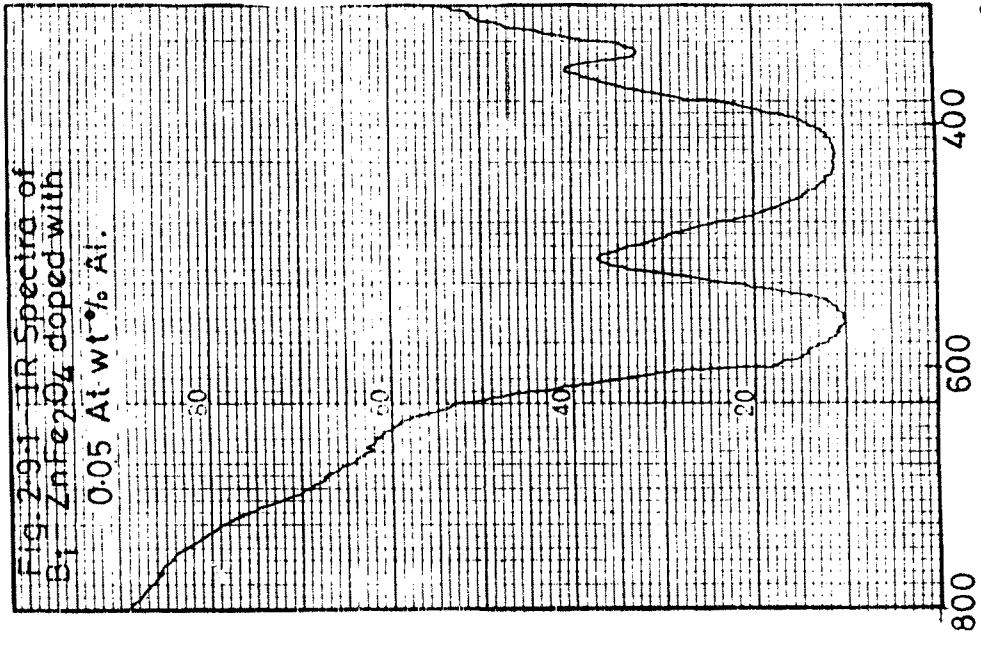
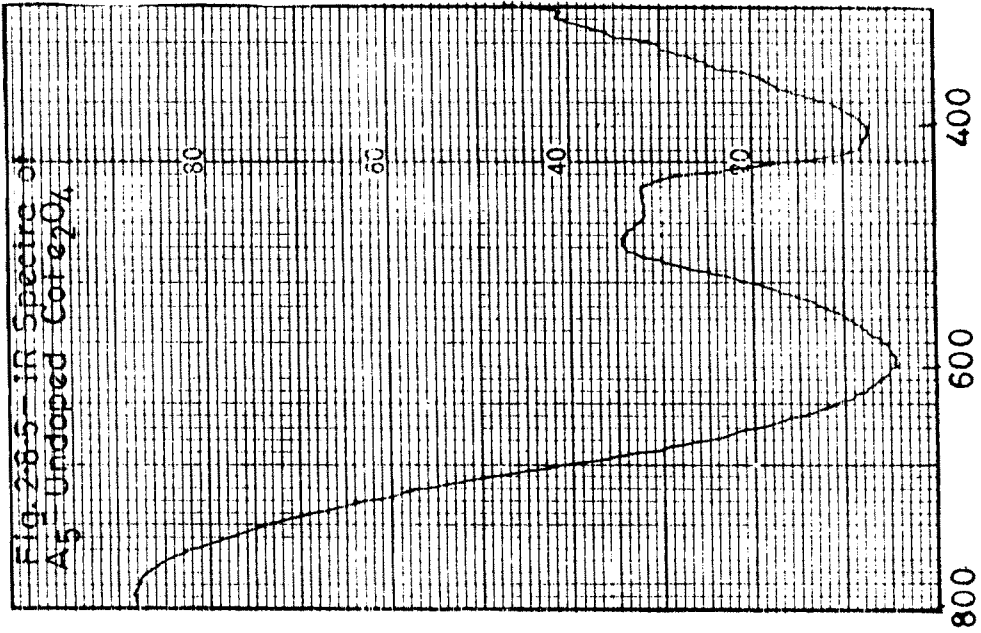
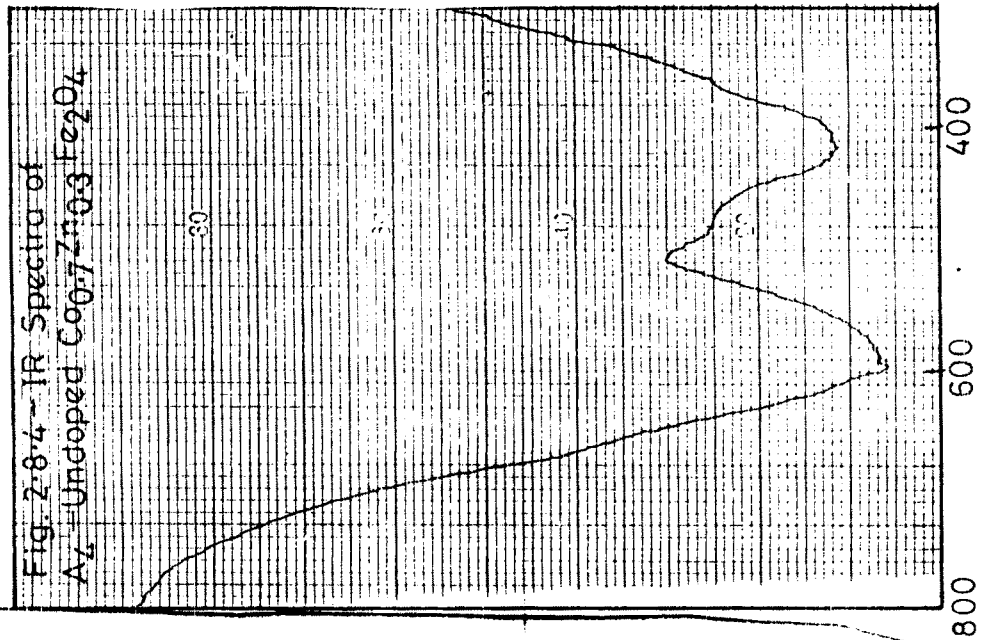
The infra red spectra were recorded at room temperature in the range of  $300\text{ cm}^{-1}$  to  $800\text{ cm}^{-1}$ . the interferometer chamber was kept under vacuum to avoid the effect of moisture of water vapour which would affect the spectrum in this region.

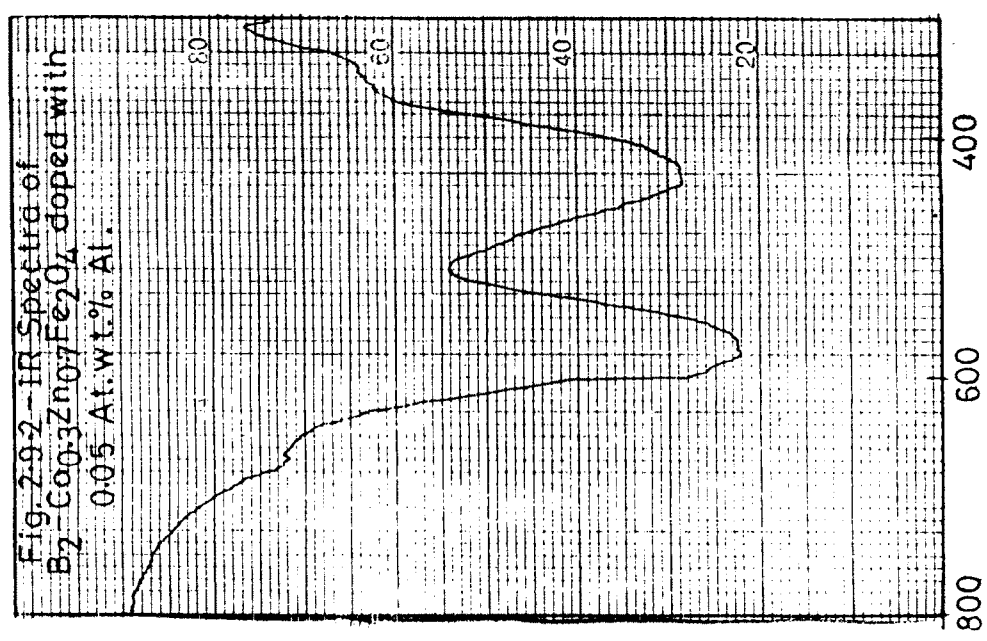
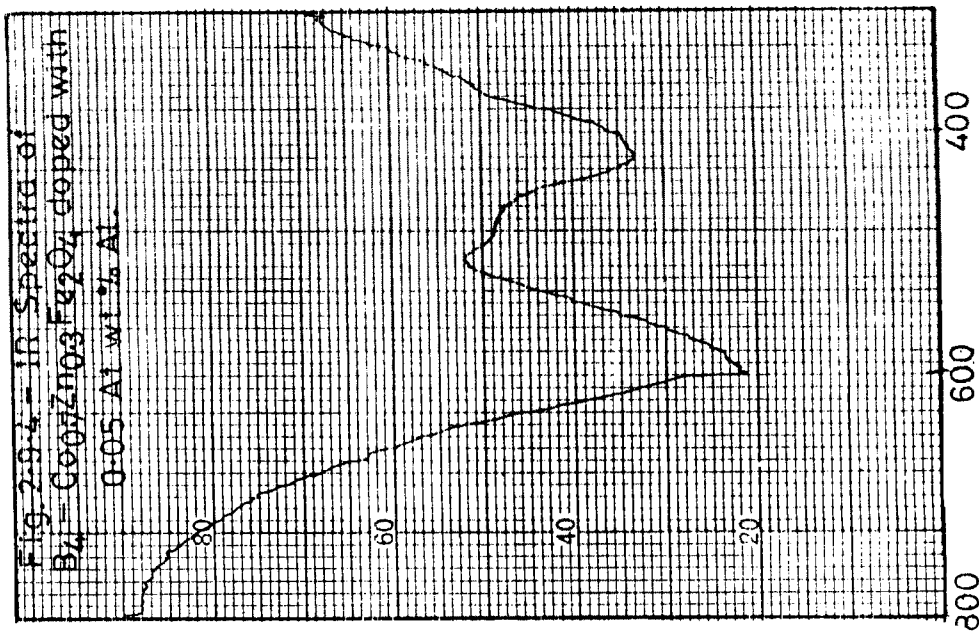
## 2.21 RESULTS AND DISCUSSIONS :

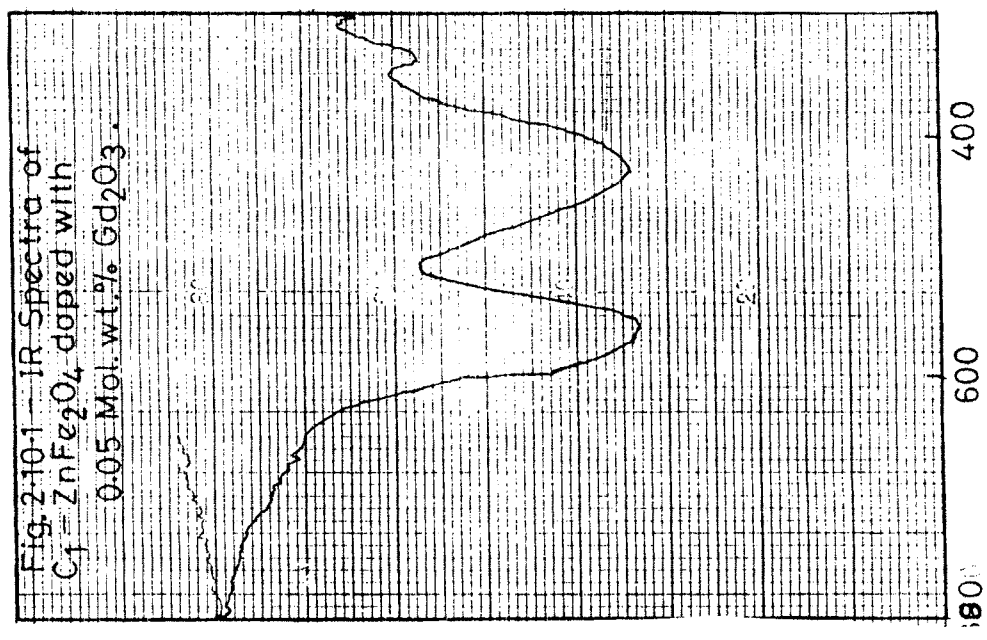
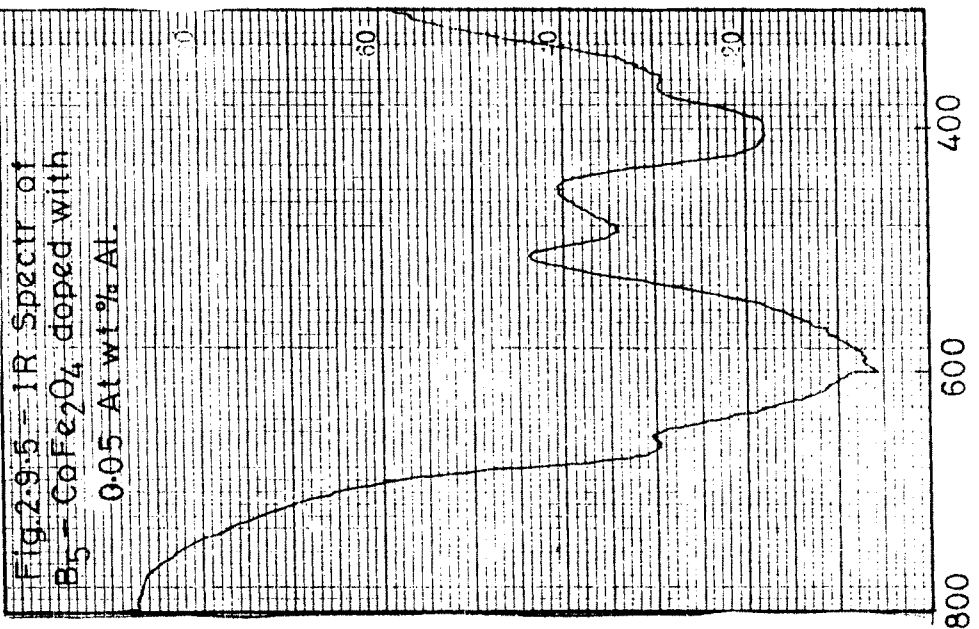
Figures 2.8.1 to 2.8.5 show the I.R. spectra of the undoped  $\text{Co}_x\text{-Zn}_{1-x}\text{Fe}_2\text{O}_4$  series. Fig.2.9.1 to 2.9.5 show the I.R.spectra of  $\text{Co}_x\text{Zn}_{1-x}\text{Fe}_2\text{O}_4$  series doped with 0.05 At. wt.% Al. Fig.2.10.1 to 2.10.5 show the I.R. spectra of  $\text{Co}_x\text{Zn}_{1-x}\text{Fe}_2\text{O}_4$  series doped with 0.05 mol. wt. %  $\text{Gd}_2\text{O}_3$ .

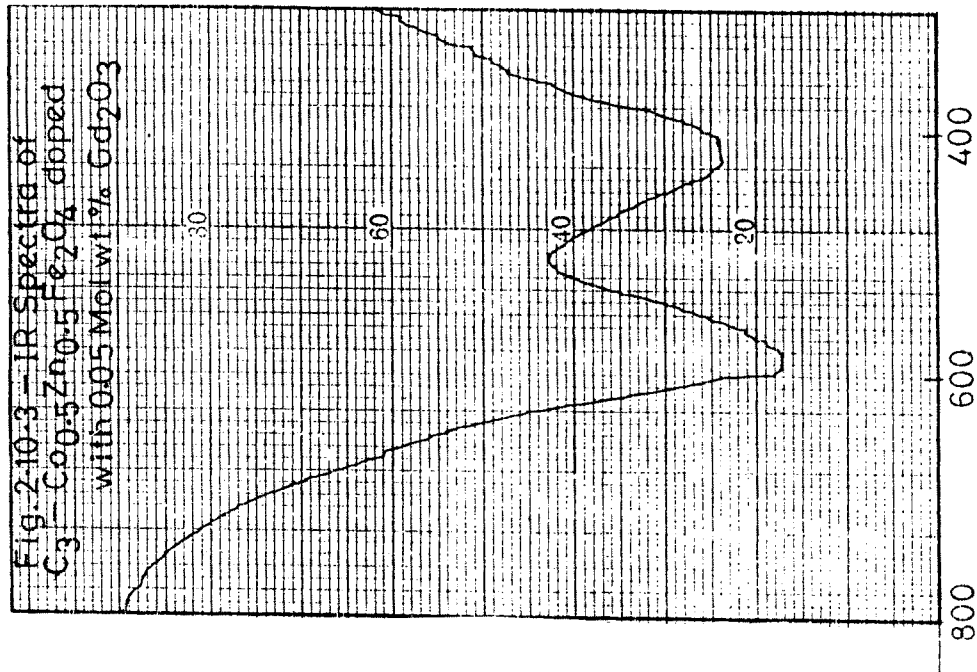
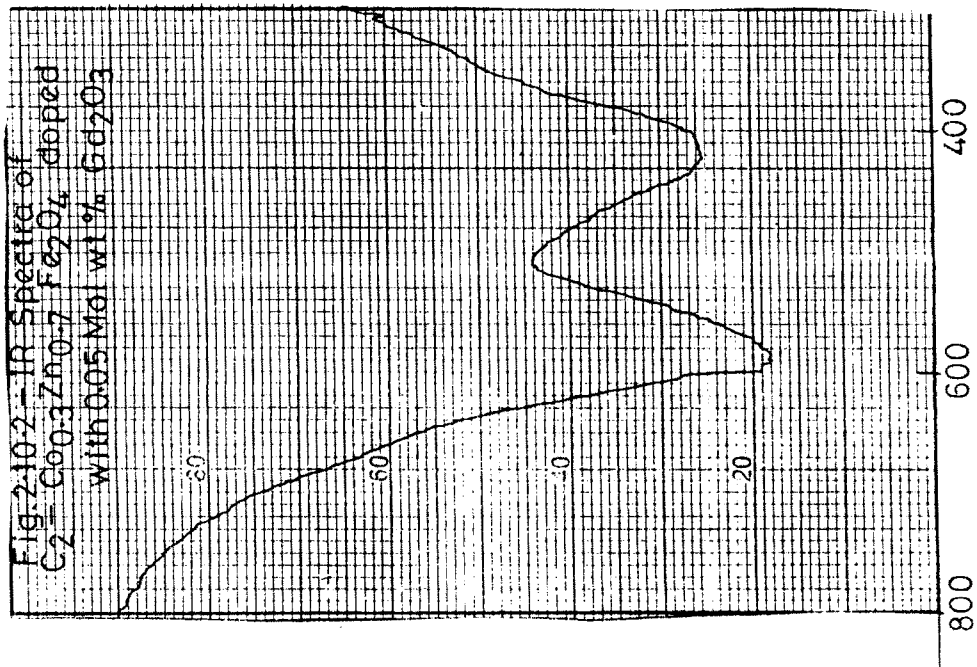
Generally it is observed that the absorption bands are broad in nature. One can observe certain structures in the absorption bands when the zinc content is varied. This structure is an indicative of the fact that changing the composition leads to creation of new absorption bands which may be attributed to the presence of specific ions. From the group theoretical classifications, it appeared that only four I.R. active modes are observed in the cubic spinel structure. For inverse and partly inverse spinels the local symmetry is distributed and the triply degenerate vibrations may split into three more vibrations. If the splitting is not too large and there is certain statistical distribution of various cations over octahedral and tetrahedral sites, one cannot observed the splitting, but only a broadening of absorption.

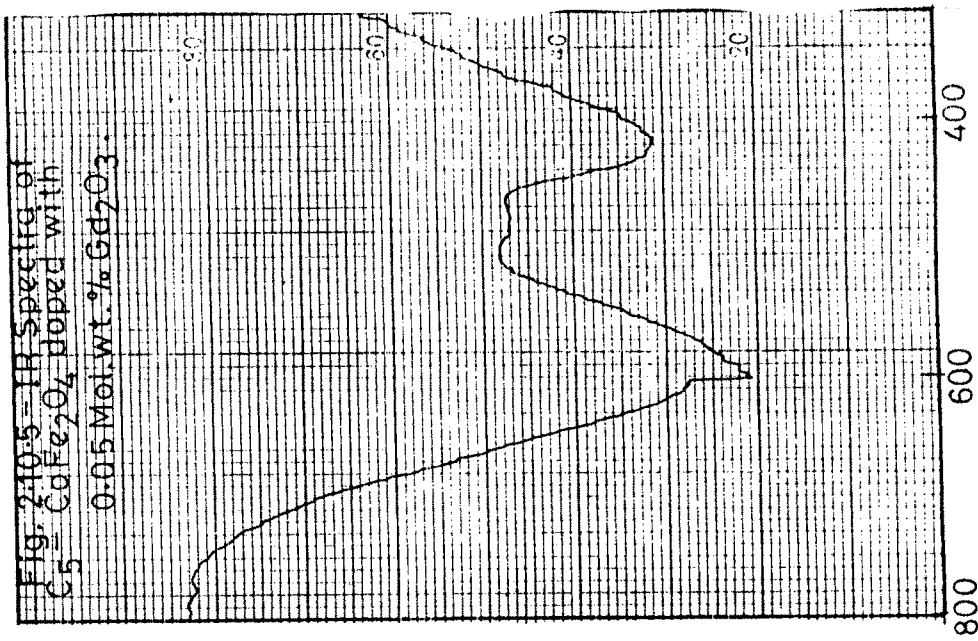
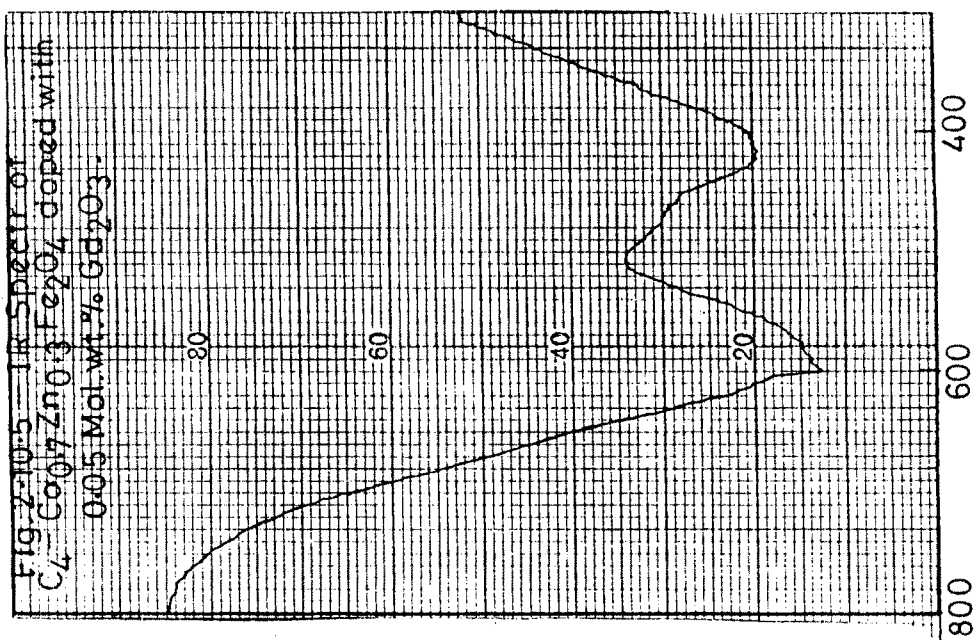












The observation of broad absorption bands in the present system may be due to this effect. Because the Cobalt ferrite is an inverse spinel whereas, zinc ferrite is normal spinel.

In the present study, the absorption bands for ferrites are found to be in the expected range. The band positions are given in Table 2.6. The high frequency band  $\nu_1$  is in the range  $550\text{ cm}^{-1}$  to  $600\text{ cm}^{-1}$ . The lower frequency band  $\nu_2$  is in the range  $410\text{ cm}^{-1}$  to  $490\text{ cm}^{-1}$ . This difference in the band position is expected, because the differences in Fe-O distances for octahedral and tetrahedral complexes from Table 2.6, it can be seen that band  $\nu_1$  and  $\nu_2$  change slightly from one mixed ferrite to other. This change is due to changes in Fe-O complexes with the increase of Cobalt concentration. Waldron<sup>23</sup> and Halfner<sup>25</sup> were amongst the earlier to study the vibrational spectra of ferrites, attributed the band around  $600\text{ cm}^{-1}$  to be intrinsic vibrations of tetrahedral complexes and  $400\text{ cm}^{-1}$  band to octahedral complexes. The frequency of tetrahedral complex  $\nu_1$  is caused by stretching of the tetrahedral metal and oxygen bond, whereas, the frequency  $\nu_2$  is caused by oxygen vibrations in the direction perpendicular to tetrahedral ion oxygen axis.

In an inverse ferrite, octahedral site is occupied  $\text{Fe}^{3+}$  and divalent ion  $\text{Me}^{2+}$ . Due to charge imbalance, oxygen ion is likely to shift towards  $\text{Fe}^{3+}$  ion, making the force constant between  $\text{Fe}^{3+}$  and  $\text{O}^{2-}$  more hence, we have expect an increase in the band



TABLE 2.6

## INFRARED ABSORPTION BANDS

Composition	without doping				with doping 0.05 At.wt.% Al.				with doping 0.05 Gd <sub>2</sub> O <sub>3</sub>				Wt.%
	$\nu_1$ cm <sup>-1</sup>	$\nu_2$ cm <sup>-1</sup>	$\nu_3$ cm <sup>-1</sup>	$\nu_4$ cm <sup>-1</sup>	$\nu_1$ cm <sup>-1</sup>	$\nu_2$ cm <sup>-1</sup>	$\nu_3$ cm <sup>-1</sup>	$\nu_4$ cm <sup>-1</sup>	$\nu_1$ cm <sup>-1</sup>	$\nu_2$ cm <sup>-1</sup>	$\nu_3$ cm <sup>-1</sup>	$\nu_4$ cm <sup>-1</sup>	
	Co <sub>0.0</sub> ZnFe <sub>2</sub> O <sub>4</sub>	560	420	340	-	560	420	340	-	560	430	340	
Co <sub>0.3</sub> Zn <sub>0.7</sub> Fe <sub>2</sub> O <sub>4</sub>	580	420	-	-	580	430	330	-	590	420	-	-	-
Co <sub>0.5</sub> Zn <sub>0.5</sub> Fe <sub>2</sub> O <sub>4</sub>	595	420	-	-	590	430	350	-	595	420	-	-	-
Co <sub>0.7</sub> Zn <sub>0.3</sub> Fe <sub>2</sub> O <sub>4</sub>	600	420	-	-	600	430	-	-	600	420	-	-	-
Co <sub>1.0</sub> Zn <sub>0.0</sub> Fe <sub>2</sub> O <sub>4</sub>	600	420	-	-	600	400	360	-	600	490	410	-	-

stretching frequency  $\nu_1$  as we go from normal to inverse spinel. These observations holds good for the present system. Similar results are also observed for Ni-Zn ferrites<sup>34,35</sup>. Similar variation is observed in case of doped series. The slight variation in the frequency for doped samples may be due to doping of impurity atoms in the lattice, which ultimately changes the Fe-O bond. Number of workers have suggested that method of preparation, grain size, porosity can be influencing factor in locating the band positions.

With the doping of Aluminium into the lattice of Cobalt-zinc ferrite system, a new band  $\nu_3$  arround  $350 \text{ cm}^{-1}$  have been noticed. Tarte<sup>24</sup> has stated that, the nature of these frequencies mainly depends on the identity of transition metal ion in octahedral sites and to a smaller extent on ions situated in tetrahedral voids of spinels.

Badrinath<sup>36</sup> has studied the I.R. spectra of  $\text{Mg Al}_{2-x}\text{Fe}_x\text{O}_4$  spinel with x varying from 1.3 to 2. He has pointed out that presence of  $\nu_3$  band is due to presence of Aluminium ions on octahedral site. Our observation show that whereas there is absence of  $\nu_3$  band in undoped samples, the same appears in corresponding Aluminium doped version. This perhaps indicate that Aluminium impurity occupies position of Fe ions on octahedral sites. This can be further supported from our observations on lattice parameter measurements. It is observed tht for Aluminium doped samples lattice parameter has been decreased though by small amount in comparis.on with undoped version as ionic radius of  $\text{Al}^{3+}$  is smaller than  $\text{Fe}^{3+}$

The  $\nu_3$  band in some compositions is not seen clearly. But the broadness and shape of the spectra suggest the possibility of its presence. The intensity of this band is increasing with the concentration of Cobalt.  $\nu_3$  band may be interpreted as the splitting of  $\nu_2$  band due to presence of impurity atom. The impurity atom causes destruction of cubic symmetry at octahedral site and hence the three fold degeneracy of  $\nu_2$  band is removed. As the Cobalt concentration in mixed ferrite system increases more and more Cobalt is transferred on B site and hence, the intensity of  $\nu_3$  band increases. For the highest concentration of Cobalt this  $\nu_3$  band can be seen clearly. So the small band  $\nu_3$  may be coming from octahedral complexes. Besides the  $\text{Fe}^{3+}$  ions in octahedral sites  $\text{Co}^{2+}$  ions are also present. The increase of Cobalt concentration causes the increase in Co-O complexes and hence increase in intensity of  $\nu_3$  band is expected and is confirmed by the results. Hence, this band  $\nu_3$  can be assigned to Co-O octahedral complexes. In other words this band can be assigned to the divalent metal ion oxygen complexes in the octahedral sites.

In Gadolinium doped samples, no splitting of  $\nu_2$  band into  $\nu_2$  and  $\nu_3$  is observed. This may perhaps be due to similarity in electronic configuration of  $\text{Gd}^{3+}$  and  $\text{Fe}^{3+}$ , as  $\text{Gd}^{3+}$  replaces one of the  $\text{Fe}^{3+}$  ion on octahedral site. Electronic configuration of  $\text{Fe}^{3+}$  is  $[\text{Ar}d^5]$  whereas, that of Gadolinium is  $[5d^{10}4f^7]$ . Whereas that of  $\text{Al}^{3+}$  is  $2P^6$  (or that of neon). From the electronic configuration of  $\text{Al}^{3+}$ ,  $\text{Gd}^{3+}$  and  $\text{Fe}^{3+}$  it can be noted that Aluminium would disturb the cubic symmetry of octahedral site to a maximum

extent whereas, Gadolinium will do so to a very little extent and hence splitting of  $\nu_2$  into  $\nu_2$  and  $\nu_3$  is observed in Al doped sample, whereas, such splitting is absent in Gd doped version.

## R E F E R E N C E S

1. Toshio Taka da ,M.Kiyama  
"Ferrite" Proc. Inc. Conf. Tokyo Japan P 61.(1970)
2. Donald G.Wickman  
"Ferrite Proc.Conf.Tokyo, Japan P-105 (July,1970)
3. Toshihiko Sata, Chinji Kuroda, Minorce Sato.  
"Ferrite" Proc. Conf. Tokyo Japan P-72 July,1970.
4. Gorter E.  
Proc.I.R.E. 42(2) 1945 (1955).
5. Bozorth R.M.  
"Ferromagnetism" P 244. (1951) Van.Nostrand,  
Netherland.
6. Vent J.J. and Gorter E.W.  
Philips Tech. Rev. 13, 181, (1952).
7. E.Hirota  
Japan J.Appl. Phys. 5-1125, (1966).
8. B.M.Yarovsky and A.A.Pinsky.  
Fundamentals of Physics Vol.I P 336-338 (1975).
9. Wagner C.Z.  
J.Phys. Che,.B-34 P 309-334.
10. Standley K.J.  
"Oxide magnetic materials" Clarendon Press New  
York Chapter 2 P.9. (1972).
11. G.Economos  
J.Am.Cer. Soc. 38, 241, (1955).

12. T.Sato  
IEEE Trans. Mag. MAG 6, 798 (1970).
13. D.Swallow, A.K. Jordon  
Proc. Brit. Ceram.Soc. 21, (1964).
14. F.R.N.Nabarrao  
Rep. Conf. Strength of solids Phy.Soc.London  
P-75, (1948).
15. C.Heirring  
J.Appl.Phys, 21. 2137, (1950).
16. C.Kittel  
"Introduction to solid state Physics"
17. P.Debye and P.Scherrer  
Physica 2, 17, 277. (1916) 18, 219 (1917).
18. A.W.Hull  
Phys. rev. 9, 84, 564 (1916). and Phy.Rev. 10,  
661, (1917).
- 19 Henry N.F.M. Lipsen H. and Wooster W.A.  
"The interpretation of X-ray diffraction photographs"  
Macmillan and Co. Ltd., London (1961).
20. Cullity B.A.  
Elements of X-ray diffraction Addison Wesley  
Pub. Inc.England (1959).
- 21 R.D.Shanon. C.T.Previtt  
Acta Cryst. B-25 925 (1969).
22. Levine B.F.  
Phy.Rev. B-7 2591, (1973).

23. Waldron R.D.  
Phys. Rev. 99 727 (1955).
24. P.Tarte  
Spectrochim Acta. 19, 49, (1963).
25. S.T,Halfner  
Z.Krist 115 331 (1961).
26. J.Prudhomme and P.Tarte  
Soelectrochim. Acta 23A 985 (1967) & 23A 1817(1971)
27. W.B.White, B A De Angelis  
Spectrochim Acta 23A 985 (1967).
28. V.R.K.Murthy ,C.Chitra Sankar, K.V. Reddy J.Sobhnadri  
Indian J.Pure and Appl.. Phys.16, 79 (1978).
29. Brabers V.A.M.  
Phys. Status Solid (Germany) Vol33/2 P 563 (1969)
30. Brabers V.A.M.  
Phys.Status Solidi a(12) 629 (1972).
31. Brabers V.A.M. and Vandenderghe R.E.  
Phys. Letters Vol. 44 A
32. Klerk J. Braber V.A.  
Solid State Comm. (USA) Vol.14/7 P.613 April  
(1974).
33. Murthy V.R.K. Chitrashankar C.Reddu K.V. Sobhnadri J.  
Indian J.Pure and App. Phys. Vol.16, 79-83(1978)
34. O.S.Josyulu and Sobhnadri J.  
Phys. Stat. Solidi (a) 59, 323, (1980)

35. O.S.Josyulu and Sobhnadri J.  
Phys. Status Solidi (a) 429, (1981).
36. K.V.S. Badrinath  
Phys. Stat. Solid (a) 91, K 19 (1985).